Research Paper

GEOSPHERE

GEOSPHERE, v. 17, no. 6

https://doi.org/10.1130/GES02410.1

8 figures; 2 tables; 1 set of supplemental files

CORRESPONDENCE:
eva.enkelmann@ucalgary.ca

CITATION: Enkelmann, E., and Falkowski, S., 2021, Deformation between the highly oblique Yakutat–North American plate boundary and the Eastern Denali fault: Geosphere, v. 17, no. 6, p. 2123–2143, https://doi.org/10.1130/GES02410.1.

Science Editor: Andrea Hampel
Associate Editor: Jeff Lee

Received 31 January 2021
Revision received 17 June 2021
Accepted 12 August 2021

Published online 27 October 2021

Deformation between the highly oblique Yakutat–North American plate boundary and the Eastern Denali fault

Eva Enkelmann[1,*] and Sarah Falkowski[2,*]

[1]Department of Geoscience, University of Calgary, Calgary, Alberta, T2N 1N4, Canada
[2]Department of Geosciences, University of Tübingen, 72076 Tübingen, Germany

ABSTRACT

This study investigates the spatial and temporal pattern of rock exhumation inboard of the highly oblique Yakutat–North American plate boundary. We aim to quantify how far deformation is transferred inboard of the Fairweather transform plate boundary and across the Eastern Denali fault. We present new detrital apatite and zircon fission track data from 27 modern drainages collected on both sides of the Eastern Denali fault and from the Alsek and Tatshenshini River catchments that drain the mountainous region between the Fairweather fault and the Eastern Denali fault. By integrating our data with published bedrock and detrital geochronology and thermochronology, we show that exhumation reaches much farther inboard (>100 km) of the Fairweather fault than farther north in the St. Elias syntaxial region (<30 km). This suggests that the entire corridor between the Fairweather and Eastern Denali faults exhumed since mid-Miocene time. The Eastern Denali fault appears to be the backstop, and late Cenozoic exhumation northeast of the fault is very limited.

INTRODUCTION

How is deformation distributed along a highly oblique continental margin? How far is deformation transferred inboard and across different terranes and sutures? We aim to address these questions by investigating the pattern of upper crustal cooling and exhumation inboard of the Yakutat–North American transform plate boundary. The active oblique subduction and collision of the Yakutat microplate drives growth of the St. Elias Mountains along the northwestern margin of the North American plate (Fig. 1). As the Yakutat microplate moves at ~50 mm/yr (Elliott et al., 2010) into southeast Alaska, the plate boundary transitions from the dextral Fairweather transform in the south into the Chugach–St. Elias thrust and the Aleutian megathrust in the north (Fig. 1).

Previous research quantifies the amount and spatial distribution of rock exhumation that is associated with the Yakutat convergence that reaches far inboard (>500 km) above the subducted Yakutat slab in the Alaska Range (e.g., Fitzgerald et al., 1995, 2014; Benowitz et al., 2011) and the Talkeetna and Chugach Mountains (e.g., Arkle et al., 2013; Enkelmann et al., 2019). Exhumation of rocks is particularly focused on constraining bends along the central and western segment of the Denali fault (e.g., Fitzgerald et al., 1995) with numerous historic strike-slip and reverse slip earthquakes recorded such as the M_W 7.9 earthquake in 2002 (Fig. 1; Eberhart-Phillips et al., 2003). The Yakutat–North American collision zone itself is equally well studied with emphasis on the Chugach–St. Elias fold-and-thrust belt (e.g., Bruhn et al., 2004; Spotila et al., 2004; Berger et al., 2008; Meigs et al., 2008; Enkelmann et al., 2010; Chapman et al., 2012; Pavlis et al., 2012) and the eastern syntaxial corner of the St. Elias Mountains (e.g., O'Sullivan and Currie, 1996; Enkelmann et al., 2009, 2015a; Bruhn et al., 2012; Grabowski et al., 2013; Falkowski et al., 2014, 2016; Schartman et al., 2019). These studies show that exhumation is spatially very limited and reaches only <30 km inboard of the plate boundary. Most of the deformation is taken up by the Yakutat microplate and its sedimentary cover. Much less is known about the long-term deformation and exhumation farther inboard of the St. Elias Mountains and particularly along the strike-slip–dominated plate boundary (McAleer et al., 2009; Spotila and Berger, 2010; Falkowski and Enkelmann, 2016; Enkelmann et al., 2017). Recent studies revealed extremely high rates of rock exhumation (2–6 mm/yr) southwest of the Fairweather fault, which was accommodated by thrust and reverse faulting along the northern (Schartman et al., 2019) and southern end of the Fairweather fault (Lease et al., 2021). These data may suggest that rock exhumation and deformation is spatially focused along the fault. However, seismic studies suggest that the entire crustal block between the Fairweather and Eastern Denali faults is undergoing distributed strain with the Eastern Denali fault acting as the deformational backstop (Choi et al., 2021).

In this study we aim to address two main questions: (1) how far does rock exhumation reach inboard (northeast) of the Fairweather transform plate boundary and does it change along strike? (2) What is the exhumation pattern across the Eastern Denali fault that separates the Insular superterrane from the Intermontane superterrane? We answer these questions by investigating the thermal history of the upper crust along the Eastern Denali fault and the regions between the Fairweather fault and the Eastern Denali fault (Fig. 1). This 120-km-wide corridor is characterized by high mountainous topography of the St. Elias Mountains (Fairweather, Alsek, and Kluane Ranges) with peaks exceeding 4000 m of elevation and large glaciers eroding material that is

Eva Enkelmann https://orcid.org/0000-0002-1988-0760
*E-mail: eva.enkelmann@ucalgary.ca; sarah.falkowski@uni-tuebingen.de

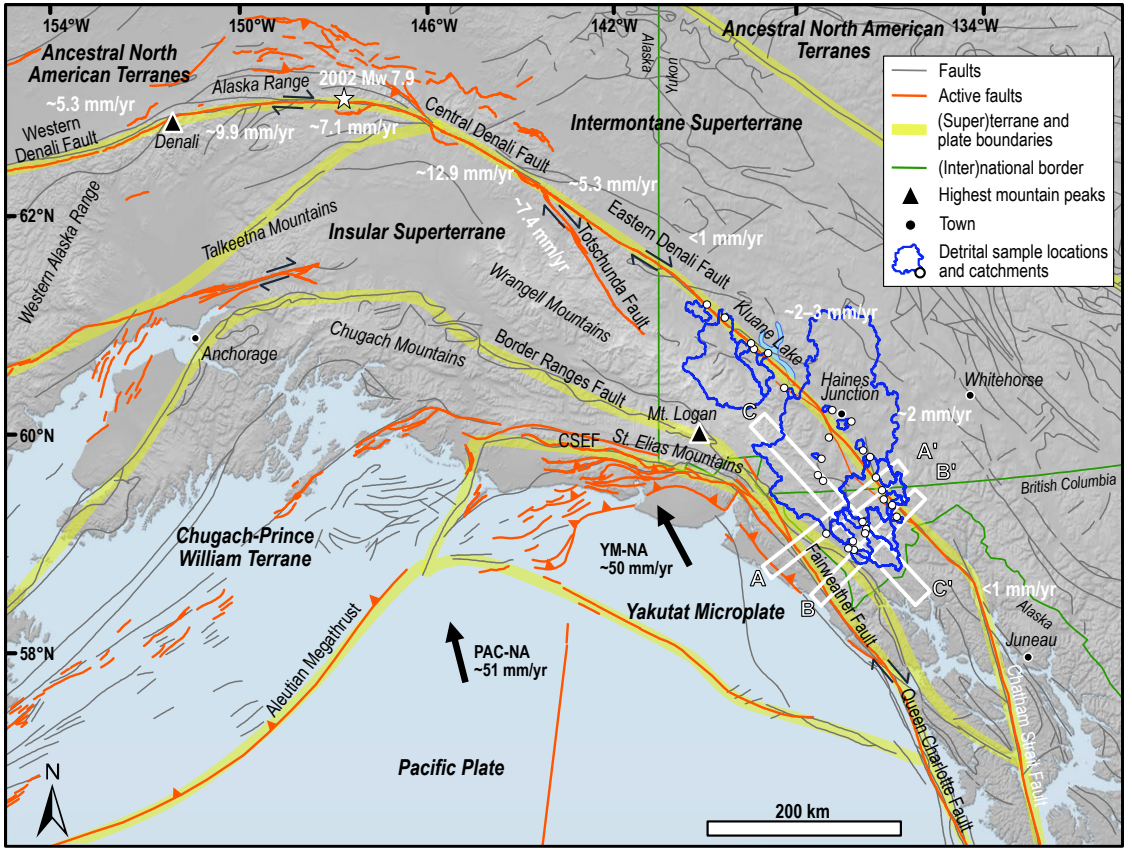

Figure 1. Topographic map (draped over hillshade based on GTOPO30) shows northwestern North America with main tectonic and geographic features. Denali is 6190 m above sea level (asl) and Mount Logan is 5959 m asl. White numbers along the Denali fault are Quaternary mean slip rates from Marechal et al. (2015, 2018), Haeussler et al. (2017), and Brothers et al. (2018). The white star marks the epicenter of the 2002 M_w = 7.9 earthquake (Eberhart-Phillips et al., 2003). Active, Quaternary (mainly for Alaska), and older bedrock faults are modified from Koehler et al. (2012) and Garrity and Soller (2009), respectively. Plate velocity vectors are after Plattner et al. (2007) and Elliott et al. (2010). PAC—Pacific plate, NA—North American plate, YM—Yakutat microplate, CSEF—Chugach-St. Elias fault. White boxes indicate the locations of three swath profiles shown in Figure 4.

mostly transported into the Gulf of Alaska by the Alsek and Tatshenshini Rivers (Fig. 2). We present 1431 new apatite fission track (AFT) and 2505 new zircon fission track (ZFT) data from 27 catchments. We use detrital thermochronology of modern glacial and fluvial deposits to infer first-order information about rock cooling occurring on catchment scales. While this analytical approach does not provide cooling information with high spatial resolution as bedrock studies do, it is the most effective method of obtaining cooling information from underneath glaciers and in inaccessible, remote regions. Detrital thermochronology studies in the St. Elias Mountain (e.g., Enkelmann et al., 2008, 2009, 2015a; Falkowski et al., 2014) and other glaciated regions such as the Alaska Range (e.g., Lease et al., 2016) showed that bedrock thermochronology alone results in a biased cooling record due to sampling of the ice-free portions of the landscape. Our new data are integrated with the published detrital ZFT and AFT data derived from the largest glacial catchments that drain the core of the St. Elias Mountains toward the north and east (Falkowski and Enkelmann, 2016) and with published bedrock thermochronology data from the area (McAleer et al., 2009; Spotila and Berger, 2010; Falkowski and Enkelmann, 2016; Enkelmann et al., 2017; McDermott et al., 2019).

GEOLOGIC AND TECTONIC SETTING

The tectonic history of the North American Cordillera is characterized by accretion since the Paleozoic (Jones et al., 1972; Coney et al., 1980). The study area is composed of terranes, including the Intermontane superterrane, against which the Insular superterrane, comprising the Wrangellia, Alexander, and Peninsular terranes, accreted in the mid Cretaceous (e.g., Rubin et al., 1990; Dusel-Bacon et al., 1993). The Eastern Denali fault separates the two superterranes (Fig. 1). North of the Eastern Denali fault, the study area is characterized by continental margin sequences that were extensively intruded by plutonic

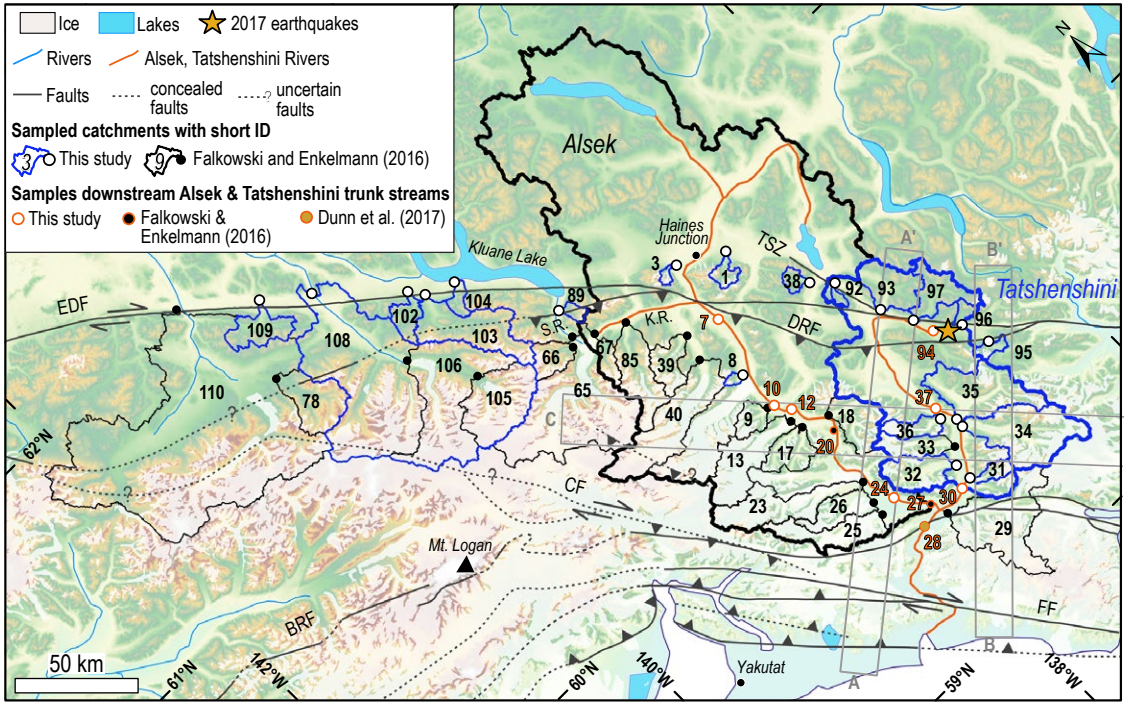

Figure 2. Topographic map (based on ASTER GDEM V3) shows the study area with outlined newly and previously studied glacial and river catchments along the Eastern Denali fault (EDF) and between the EDF and Fairweather fault (FF). Thin black and blue lines are boundaries of individual catchments for a sample; bold black and blue lines are outlines of the entire catchment for the Alsek and Tatshenshini Rivers. Note that KLD has been dropped from sample IDs. Gray boxes indicate locations of swath profiles shown in Figure 4 (see Fig. 1 for the full extent of profile C-C'). Faults were simplified after Wilson et al. (2015), Spotila and Berger (2010), and Falkowski and Enkelmann (2016). DRF—Duke River fault, TSZ—Tatshenshini Shear Zone, CF—Contact fault, BRF—Border Ranges fault, S.R.—Slims River, K.R.—Kaskawulsh River.

rocks of the Kluane Arc (ca. 85–45 Ma). The Kluane Arc is part of the Coast Plutonic Complex and is represented in the study area by the Paleocene–early Eocene Ruby Range Batholith (e.g., Armstrong, 1988; Erdmer and Mortensen, 1993). Geochronology and high-temperature thermochronology ages (57–40 Ma) of the intruded Kluane Metamorphic Schist are interpreted as having cooled due to rapid uplift following intrusion (Erdmer and Mortensen, 1993), which is supported by sparse low-temperature thermochronologic data in the area (Enkelmann et al., 2017). Furthermore, metasedimentary rocks of a Late Jurassic–Early Cretaceous flysch basin (Dezadeash Formation of the Gravina-Nutzotin belt; e.g., Berg et al., 1972; Eisbacher, 1976; Lowey, 1992) are displaced along the Eastern Denali fault (Fig. 3). These sediments have been deformed and metamorphosed in association with the mid–Late Cretaceous final accretion of the Insular superterrane (e.g., Dusel-Bacon et al., 1993). The Denali fault may have accommodated up to 400 km of dextral displacement over the Cenozoic (Lowey, 1998). Details about the Cenozoic slip history, and possibly varying slip amounts between the eastern and western fault segments, remain uncertain (e.g., Regan et al., 2020).

South of the Eastern Denali fault, basement rocks of the Wrangellia and Alexander terranes comprise Paleozoic–early Mesozoic arc-backarc assemblages (e.g., Nokleberg et al., 1994). These rocks have been intruded by Jurassic–Cretaceous magmatism (ca. 160–130 Ma Chitina Arc and ca. 120–105 Ma Chisana Arc; Dodds and Campbell, 1988), which migrated northward through time (Fig. 3). Furthermore, in the Eastern Denali fault and Duke River fault zone, latest Eocene–Oligocene fluvial and lacustrine sediments of the Amphitheatre Formation were deposited in small, fault-bounded, transpressional and transtensional basins (Fig. 3; e.g., Eisbacher and Hopkins, 1977; Ridgway et al., 1992; Ridgway and DeCelles, 1993a, 1993b). These sediments are overlain by early–mid-Miocene Wrangell volcanics (Skulski et al., 1991, 1992). Wrangell volcanics and shallow intrusions of 26–0 Ma age (Richter et al., 1990; Trop et al., 2012) formed due to the passage of the Yakutat slab edge but are mostly located to the west of the study area (Wrangell Mountains in Fig. 1; Richter et al., 1990; Brueseke et al., 2019). To the south, the Insular superterrane is bounded by the Border Ranges fault. Subduction at the Insular superterranes' outboard margin continued during Cretaceous–Paleocene time (the Chugach-Prince William terrane represents the accretionary complex; Fig. 1) until a spreading-ridge subducted and the transform margin was established in the mid Eocene (Fig. 1; Fairweather–Queen Charlotte fault system; e.g., Dumoulin, 1988; Plafker et al., 1994; Haeussler et al., 2003; Pavlis and Roeske, 2007).

Since the late Eocene, the oceanic plateau of the Yakutat microplate has been translated northwestward into the St. Elias syntaxis (Figs. 1–2; e.g., Plafker,

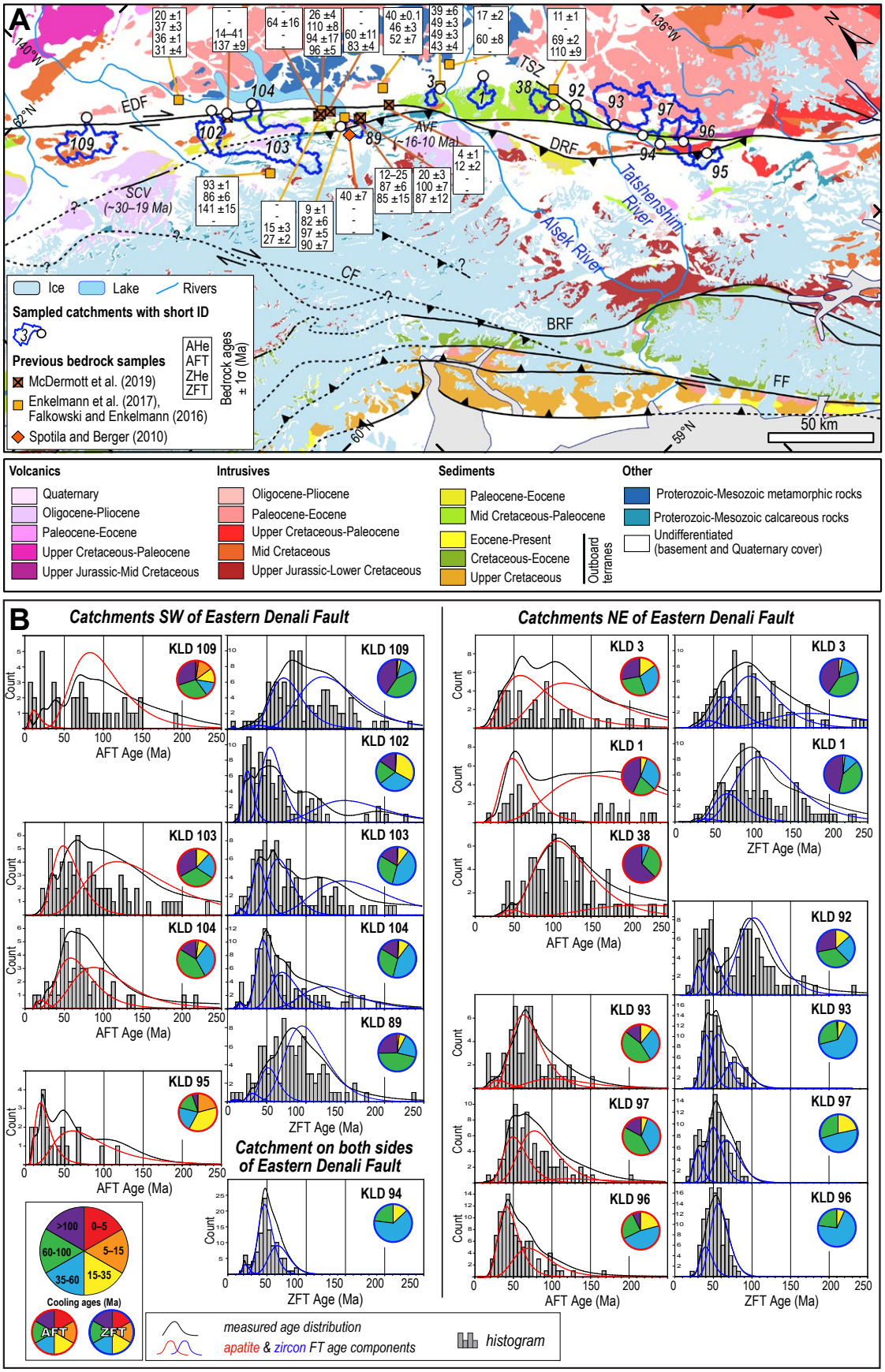

Figure 3. (A) Geologic map of the study area with outlined catchments located along the Eastern Denali fault (EDF) is shown. Note that other catchments and sample locations of this study are not shown here for clarity. Previously published bedrock low-temperature thermochronometric data from the vicinity of the sampled catchments are shown. AHe—apatite (U-Th)/He, AFT—apatite fission-track, ZHe—zircon (U-Th)/He, ZFT—zircon fission-track. TSZ—Tatshenshini Shear zone; DRF—Duke River fault; FF—Fairweather fault; CF—Contact fault; BRF—Border Ranges fault; SCV—Sonya Creek Volcanic Field (Berkelhammer et al., 2019), AVF—Alsek Volcanic Field (13.5–10.8 Ma (Stevens et al., 1982; Dodds and Campbell, 1988) and 16.4–15.4 Ma (Trop et al., 2012)). Geology is from Yukon Geological Survey (Bedrock Geology Data set, http://data.geology.gov.yk.ca/Compilation/3#InfoTab, downloaded April 2019), British Columbia Geological Survey (Cui et al., 2017), and U.S. Geological Survey (Wilson et al., 2015). Faults are simplified after Spotila and Berger (2010), WIlson et al. (2015), and Falkowski and Enkelmann (2016). (B) Histograms, probability density plots, and age component fitting curves of detrital apatite and zircon fission track (AFT and ZFT) data are shown with pie charts representing single-grain ages. The age component curves are from Binomfit software (Brandon, 1992, 1996); where two or more curves are present, they represent P1, P2, etc., as recorded in Tables 2 and S1 (see footnote 1).

1987; Finzel et al., 2011; Worthington et al., 2012). The St. Elias syntaxis, where transform motion transitions into collision and flat-slab subduction, is characterized by the highest peaks (e.g., Mt. Logan at 5959 m) surrounded by the Kluane icefield (Figs. 1–2).

The main structures in our study area are the Eastern Denali fault and the Duke River fault. The Denali fault is active and characterized by slip partitioning (e.g., Riccio et al., 2014; Bemis et al., 2015). Quaternary mean slip rates along its western and central segments in Alaska are much higher (5–13 mm/yr; Haeussler et al., 2017) than along the eastern segment in Canada (~2 mm/yr or <1 mm/yr; Fig. 1; Haeussler et al., 2017; Marechal et al., 2018). The Denali fault is capable of producing large earthquakes, such as the 2002 M_w 7.9 earthquake that ruptured hundreds of kilometers along the central Denali fault and into the Totschunda fault (Fig. 1; Eberhart-Phillips et al., 2003). The Duke River fault is a reactivated suture and thrusts Alexander terrane rocks over Wrangellia terrane rocks (Cobbett et al., 2017). Evidence for its activity and ~10–13 km of vertical motion comes from tectono-stratigraphic reconstructions, muscovite growth ages (105–79 Ma), deformation of Miocene lava and intrusions (post-15 Ma deformation), and current seismicity and crustal motion (Power, 1988; Kalbas et al., 2008; Doser, 2014; Marechal et al., 2015, 2018; Cobbett et al., 2017; Choi et al., 2021). This indicates that the Duke River fault has been reactivated due to its favorable orientation to the Yakutat-North American collision and accommodates some contractional deformation in the transpressional stress field similar to the Alaskan segments of the Denali fault zone (e.g., Bemis et al., 2015). Overall, it is important to point out that the surface geology in the study area is not well mapped due to glacial coverage, remoteness, and lack of economic interests (e.g., most of the region is part of a national or provincial park).

TABLE 1. GEOGRAPHIC INFORMATION FOR DETRITAL SAMPLES

Sample number	Latitude	Longitude	Elevation (m)	Catchment area (km²)	Catchment elevation range (m)
KLD 01	60.6735	–137.3717	801	84	801–2444
KLD 03	61.0724	–137.7053	617	27	617–2558
KLD 07	60.5238	–137.8043	546	12,973	546–4402
KLD 08	60.3256	–137.9816	515	26	515–2307
KLD 10	60.1645	–138.0214	461	14,393	461–4402
KLD 12	60.1094	–137.9185	428	16,189	428–4402
KLD 24	59.6148	–137.9056	203	18,463	203–4402
KLD 30	59.4620	–137.5219	211	5713	211–2719
KLD 31	59.4649	–137.4162	310	85	310–2671
KLD 32	59.5193	–137.4153	275	334	275–2302
KLD 34	59.6067	–137.1946	349	803	349–2719
KLD 35	59.6394	–137.1807	362	670	362–2574
KLD 36	59.6976	–137.2318	410	160	410–2425
KLD 37	59.7158	–137.2253	400	2848	400–2716
KLD 38	60.3628	–137.1519	795	66	795–2200
KLD 89	60.9785	–138.5453	813	53	813–2663
KLD 92	60.2921	–137.0246	743	32	743–1981
KLD 93	60.1107	–136.9301	724	364	724–2142
KLD 94	59.9110	–136.7999	858	237	858–2204
KLD 95	59.7337	–136.5922	960	62	960–2055
KLD 96	59.8430	–136.6532	881	59	881–2102
KLD 97	59.9917	–136.8431	835	317	835–2265
KLD 102	61.4309	–139.2208	843	158	843–2620
KLD 103	61.3741	–139.1476	860	658	860–3015
KLD 104	61.4919	–138.9333	815	79	815–2467
KLD 108	61.6772	–139.7513	680	4289	680–5035
KLD 109	61.7978	–140.0482	730	279	730–2284

Note: Coordinates in WGS84. Elevation ranges from ASTER 30 m digital elevation model.

METHODS

Sampling Modern Catchments

Studying the St. Elias Mountains is challenging due to the remoteness and extensive glaciation, which limits access to bedrock sampling. Detrital thermochronology studies on fluvial and glacial sand deposits are very effective in revealing the spatial pattern of rock exhumation and complementing bedrock studies (e.g., Enkelmann et al., 2008, 2009; Falkowski et al., 2014). The use of multiple thermochronologic systems on the same sample can provide additional information about cooling through a larger temperature window (Enkelmann et al., 2015a; Falkowski and Enkelmann, 2016). We followed this analytical approach and collected 27 sand samples from glacio-fluvial and fluvial catchments located along the Eastern Denali fault as well as from tributaries and the main streams of the Alsek and Tatshenshini Rivers in southwestern Yukon and northwestern British Columbia (Figs. 1–2; Table 1). At each location, we grabbed sand from ~50–100-m-long stretches along the riverbank or sand bar to obtain ~5 kg of a mixed medium- to coarse-grained sample. Sampling locations along the Eastern Denali fault were chosen according to hiking access from the highway that parallels the fault. We aimed to sample the small catchments that drain the fault-proximal mountains.

We collected samples along the Alsek and Tatshenshini Rivers and their tributaries using helicopter access (Fig. 2). Large glacier systems drain into the Alsek River from the northwest, for which detrital AFT and ZFT data were published by Falkowski and Enkelmann (2016) and bedrock thermochronology data by Enkelmann et al. (2017). For this study, we sampled along the Alsek trunk river and smaller tributaries of the Alsek River to obtain the cooling record of the more outboard portions (north and east) of the St. Elias Mountains. Note that samples were collected in 2012 in settings influenced by the abrupt drainage reorganization by the retreat of the Kaskawulsh Glacier

(catchment KLD 65 in Fig. 2) (Shugar et al., 2017). Before 2016, the majority of the Kaskawulsh Glacier was drained via the Slims River (S.R. in Fig. 2) and Kluane Lake in the Yukon catchment into the Bering Sea, whereas it is now mostly drained via Kaskawulsh (K.R. in Fig. 2) and Alsek Rivers into the Pacific Ocean. Therefore, the samples that were collected along the Alsek trunk (KLD 7, KLD 10, KLD 12, and KLD 24; and previous samples KLD 20, KLD 27, and KLD 28; Falkowski and Enkelmann, 2016; Dunn et al., 2017) represent the pre-2016 drainage pattern. Note that all glacio-fluvial sand samples were collected in highly dynamic settings that were influenced by glacial and climate dynamics and subject to changes in drainage patterns or sediment storage (e.g., glacial lake damming and outbursts). Along the Tatshenshini River, we sampled the trunk and tributaries that drain both sides of the river (Fig. 2). The Tatshenshini River is sourced east of the Eastern Denali–Duke River fault zone and flows to the northwest in the Eastern Denali fault zone before making a wide turn and flowing south for ~200 km through the mountainous region inboard of the Fairweather plate boundary and into the Pacific Ocean (Fig. 2). The Tatshenshini River cuts through mountains with peaks of >2500 m elevation, and many of them host alpine glaciers (Fig. 2).

Detrital Apatite and Zircon Fission Track Analyses

Samples were collected for detrital AFT and ZFT analyses. Mineral separation was conducted according to standard protocols at the University of Tübingen, Germany, and fission-track analyses were conducted at the University of Cincinnati, Ohio, USA. Details on mineral separation and the fission-track dating procedure can be found in Enkelmann et al. (2015a) and Falkowski and Enkelmann (2016). For each sample and dating method, we aimed to analyze ~100 single grains using the external detector method and ζ calibration for age determination (Hurford, 1990).

Detrital thermochronology has the advantage that it provides integrated cooling information of the bedrock within a catchment. The interpretation of detrital fission track data is based on consideration of the entire age distribution rather than on individual grain ages. However, for the resulting age distribution to be a true representation of cooling recorded by the bedrock underlying the catchment, several assumptions must be valid: (1) all lithologies within the catchment contain the accessory mineral being analyzed (e.g., apatite and zircon); (2) the mineral yield is similar for all lithologies; and (3) every lithology in the catchment is equally eroding and is equally represented in sediment carried by rivers or glaciers. Most of these assumptions are not true for catchments containing various lithologies, geologic units, and structures. For example, mineral separation of magmatic, metamorphic, and sedimentary rocks regularly results in large variations in apatite and zircon yields, and often only one or none of the accessory minerals is present. Furthermore, fault and fracture zones are regions of rock weakness and are much easier to erode; thus, they contribute more sediment than unfractured rock units. In glacial settings, the varying coverage and flow of ice results in differential erosion within the catchment, which biases the detrital record (Ehlers et al., 2015). Therefore, it cannot be simply assumed that a detrital age distribution represents the bedrock cooling of the entire catchment and that the AFT and ZFT age distributions of the same detrital sample represent the cooling of the same bedrock underlying a catchment. Despite these limitations, the resulting AFT and ZFT age distributions provide valuable first-order information on cooling recorded within a catchment, but they do not necessarily represent the complete cooling record of all rocks within the entire catchment. Detrital thermochronology was particularly successful in revealing the youngest age components in glacial catchments that are commonly missed in bedrock studies due to their bias to higher-elevation sample locations (e.g., Grabowski et al., 2013; Ehlers et al., 2015; Enkelmann and Ehlers, 2015).

RESULTS

From a total of 27 detrital samples, we present 2505 ZFT single-grain ages from 24 samples and 1431 AFT single-grain ages from 19 samples. From the measured single-grain age distribution, we extract age components using a binomial peak-fitting procedure (software BINOMFIT; Brandon, 1992, 1996). This procedure generates component distributions in the probability density plot with Gaussian-shaped peaks, and the area beneath each peak represents the proportional size of the age component (Brandon, 1996). The component age peaks (P1, P2, P3…) are reported as mean age, width (1σ), and size (percentage of grains) and are used for geologic interpretation (Table 2; e.g., Brandon et al., 1998; Garver et al., 1999). Note, from here on we use "grain ages" and "AFT/ZFT dates" when referring to the measured single-grain data and we use "age components" when referring to the peak fitting results as listed in Table 2.

AFT and ZFT age components of the 27 new samples and previously published results of 21 samples from catchments that drain the St. Elias syntaxis area toward the north and east (Fig. 2; Falkowski and Enkelmann, 2016) are reported in the Supplemental Material (Table S1[1]). All new single-grain ages and analytical details can be found in Table S2 (see footnote 1). The measured age distributions and extracted age components are visualized in probability density plots and histograms (Fig. 3). We also present the measured single-grain data in pie charts grouped into six age bins of different colors (Fig. 3). The age bins are selected to capture cooling caused by the various exhumational and magmatic phases reported from the Yakutat–North American collision zone. The youngest age bin (<5 Ma, red) represents the extremely rapid exhumation that is localized underneath the ice fields at the St. Elias syntaxis region (e.g., Enkelmann et al., 2009; Falkowski et al., 2014). The 5–15 Ma age bin (orange) captures the time since the beginning of the Yakutat collision, which resulted in accelerated rock exhumation within both the Yakutat and North American plates (Grabowski et al., 2013; Enkelmann et al., 2017). The 15–35 Ma age bin (yellow) captures the rock exhumation associated with the northwestward translation of the Yakutat microplate along the transform boundary, which results in flat slab subduction underneath southern Alaska (e.g., Finzel et al.,

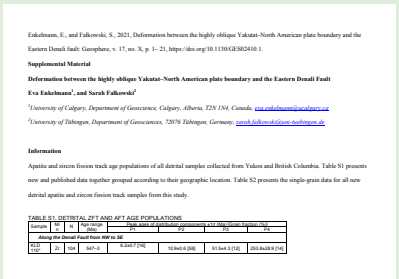

Enkelmann, E., and Falkowski, S., 2021, Deformation between the highly oblique Yakutat–North American plate boundary and the Eastern Denali fault: Geosphere, v. 17, no. X, p. 1– 21, https://doi.org/10.1130/GES02410.1.

Supplemental Material

Deformation between the highly oblique Yakutat–North American plate boundary and the Eastern Denali Fault

Eva Enkelmann[1], and Sarah Falkowski[2]

[1]*University of Calgary, Department of Geoscience, Calgary, Alberta, T2N 1N4, Canada,* eva.enkelmann@ucalgary.ca

[2]*University of Tübingen, Department of Geosciences, 72076 Tübingen, Germany,* sarah.falkowski@uni-tuebingen.de

Information

Apatite and zircon fission track age populations of all detrital samples collected from Yukon and British Columbia. Table S1 presents new and published data together grouped according to their geographic location. Table S2 presents the single-grain data for all new detrital apatite and zircon fission track samples from this study.

TABLE S1. DETRITAL ZFT AND AFT AGE POPULATIONS

Sample	N*	N	Age range (Ma)	Peak ages of population components ±1.1σ (Mixture Fission Track)			
				P1	P2	P3	P4
Along the Denali Fault from NW to SE							
KLD 109	20	194	647–3	4.2±0.7 [19]	10.8±0.6 [68]	61.5±4.3 [13]	253.8±28.8 [19]

[1]Supplemental Material. All peak fitting results from this study and previously published catchments (Table S1) and the single-grain data of the new data (Table S2). Please visit **https://doi.org/10.1130/GES.S.15161556** to access the supplemental material, and contact editing@geosociety.org with any questions.

TABLE 2. DETRITAL ZFT AND AFT AGE COMPONENTS

Sample	Min	N	Age range (Ma)	Age components ±1σ (Ma) [Grain fraction (%)]			
				P1	P2	P3	P4
Along the Eastern Denali Fault from northwest to southeast							
KLD 109	Zr	104	223–7	7.3±1.8 [1]	38.4±11 [3]	71.2±6.9 [45]	121.4±11 [51]
	Ap	40	570–5	11.0±1.8 [25]	82.6±5.5 [75]		
KLD 108	Zr	105	313–4	5±1.1 [2]	7.2±1.2 [1]	69.4±7.8 [32]	132.5±11 [65]
KLD 102	Zr	105	325–11	25.3±2.1 [34]	54.3±4.5 [49]	148.6±15 [17]	
KLD 103	Zr	104	384–11	17.2±2.4 [4]	39.2±3.5 [30]	64.3±5.6 [37]	147.2±13.6 [30]
	Ap	67	311–22	48.3±3.3 [50]	116.7±11 [50]		
KLD 104	Zr	105	317–10	15.1±1.9 [5]	45±3.7 [48]	69.3±9.5 [28]	124±13 [19]
	Ap	50	357–14	20.4±3.4 [7]	58.2±7.4 [51]	87.2±13.5 [42]	
KLD 89	Zr	104	224–6	9.3±2.1 [3]	31.7±4.8 [6]	51.6±4.9 [25]	94.8±7.5 [66]
KLD 03	Zr	104	25–300	42.8±8.4 [7]	64.8±9.2 [27]	97±12.2 [49]	172±27 [16]
	Ap	50	4–329	9.8±11 [5]	58.1±7 [55]	120.7±13 [40]	
KLD 01	Zr	103	26–251	41.4±11.5 [3]	67.0±8.2 [26]	108.7±9.6 [72]	
	Ap	35	20–284	48.2±4.2 [52]	153.8±18 [48]		
KLD 38	Ap	93	36–350	47.4±5.5 [5]	105.2±5.6 [80]	215.6±38 [15]	
KLD 92	Zr	104	18–230	30.6±2.6 [17]	48.9±4.2 [26]	103±7.8 [57]	
KLD 93	Zr	103	28–100	40.4±3.3 [40]	55.6±5.4 [40]	77.5±7 [20]	
	Ap	63	19–151	23.4±5.5 [5]	44.7±11 [15]	68.6±4.2 [80]	
KLD 97	Zr	105	20–93	29.5±2.4 [24]	50.0±5.1 [41]	66.6±6.8 [35]	
	Ap	77	17–198	49.6±3.7 [44]	77.2±7.8 [51]	120.2±52 [5]	
KLD 96	Zr	105	23–80	39.9±3.8 [29]	56.3±4.3 [71]		
	Ap	100	21–399	41.0±2.1 [70]	69.6±6.4 [30]		
KLD 95	Ap	19	9–116	18.8±2.6 [62]	59.4±12 [38]		
Tatshenshini River catchment							
KLD 94	Zr	105	19–86	22.3±2.1 [9]	46.8±3.7 [64]	63.7±6 [27]	
KLD 37	Ap	101	5–153	17.1±3.5 [12]	42.2±3.3 [72]	66.6±10 [16]	
KLD 36	Zr	104	58–191	80.1±6.7 [43]	108±16 [30]	142.9±16.7 [27]	
	Ap	67	2.2–107	13.3±1.2 [69]	49.7±11.5 [31]		
KLD 35	Zr	104	17–138	23.7±2 [22]	34.5±2.7 [55]	54.9±4.6 [16]	100.3±9.3 [7]
KLD 34	Zr	105	25–212	40.7±4.2 [9]	105.9±7.5 [91]		
	Ap	103	2–114	13.7±2.2 [42]	25.4±5 [47]	46.3±10 [11]	
KLD 32	Zr	105	49–186	68.7±9 [13]	102.1±8.4 [79]	146±28 [8]	
	Ap	102	4.5–99	15.5±2.5 [44]	26.8±6 [42]	59.8±8.5 [14]	
KLD 31	Zr	104	27–164	34.6±3.6 [11]	67.9±6 [43]	98.6±8.3 [47]	
	Ap	105	3.5–126	12.9±2.8 [23]	23.2±3.9 [49]	43.8±5.5 [28]	
KLD 30	Zr	105	52–245	75.3±7.6 [19]	115.7±9.2 74]	187.8±28 [7]	
	Ap	105	4–84	14.6±2 [64]		39.2±3.8 [36]	
Alsek River catchment							
KLD 07	Zr	105	1–183	4.6±0.7 [19]	9±1 [21]	88.7±6.9 [60]	
	Ap	72	2.7–197	12.7±1.4 [51]	95.1±5.8 [49]		
KLD 08	Zr	104	26–255	39.8±5.8 [6]	87.1±10.5 [35]	125.2±11.3 [59]	
KLD 10	Zr	105	22–293	36.5±3.3 [16]	69±5.5 [59]	133.9±12.5 [25]	
	Ap	75		49.2±8.9 [4]	104.1±6.3 [61]	134.8±25 [35]	
KLD 12	Zr	103	48–247	74.1±6.6 [32]	121.8±9.8 [68]		
KLD 24	Zr	105	4–224	5.8±1.4 [3]	72.1±8.7 [21]	121.1±10 [76]	
	Ap	107	3.4–201	11.3±0.8 [51]	28.1±2.6 [25]	99.6±7 [24]	

Note: Results of binomial peak-fitting using Binomfit (Brandon, 1992, 1996). Min—mineral; Zr—zircon; Ap—apatite; N—number of single grains dated per sample. A complete list of all published and new detrital apatite fission track (AFT) and zircon fission track (ZFT) age component results are in Table S1 (see footnote 1). Single-grain data of this study are given in Table S2 (see footnote 1).

2011; Falkowski et al., 2014). The 35–60 Ma age bin (blue) captures the time of late Paleocene–Eocene near-trench magmatism and metamorphism that resulted in the Chugach Metamorphic Complex and was followed by tectonic plate reorganization (e.g., Hudson and Plafker, 1982; Haeussler et al., 2003; Gasser et al., 2011). The two oldest age bins, which are 60–100 Ma (green) and >100 Ma (purple), capture the time of subduction along the western margin of North America. The younger age bin represents mostly the Late Cretaceous–Paleocene Coast Plutonic Complex, while the oldest age bin represents the magmatism associated with the formation of the Chitina and Chisana Arcs (e.g., Dodds and Campbell, 1988; Dusel-Bacon et al., 1993).

In general, the age distributions are composed of two to four age components with peaks ranging from ~10–215 Ma for apatite and ~5–190 Ma for zircon (Table 2). Overall, ZFT age components are similar to or older than AFT age components (within 1σ error) as would be expected from the higher closure temperature of ZFT (~250 °C; Brandon et al., 1998) compared to that of AFT (~110 °C; Ketcham et al., 1999). However, there are also a few samples with younger ZFT than AFT age components (e.g., samples KLD 97 and KLD 103; Table 2). The most likely explanation for such age inversion is a heterogeneous mineral yield in the catchments due to variable lithologies and possible non-uniform erosion patterns that result in variable contributions of grains from different regions. The following description of our results is subdivided into two areas: (1) catchments along the Eastern Denali fault and (2) catchments between Eastern Denali fault and Fairweather fault (Fig. 2).

Detrital AFT and ZFT Cooling Record along the Eastern Denali Fault

A total of 14 samples were analyzed from both sides of the Eastern Denali fault (Fig. 3). For samples KLD 89, KLD 92, KLD 94, and KLD 102 we only obtained ZFT results, and for samples KLD 38 and KLD 95 only AFT results were obtained. The remaining eight samples yielded ZFT and AFT data. ZFT age components have peaks ranging between 25.3 ± 2.1 Ma (34%) and 172.0 ± 27.0 Ma (16%), while AFT components have peaks ranging from 11.0 ± 1.8 Ma (25%) to 215.6 ± 38.0 Ma (15%; Table 2). Age components that comprise <5% of measured grains are not considered to be statistically significant (Vermeesch, 2004) and are not further discussed here, but they are reported in Tables 2 and S1 (footnote 1). All measured age distributions are relatively wide with the exception of samples KLD 92, KLD 93, KLD 96, and KLD 97, which are located northeast of the Eastern Denali fault or overlap the Eastern Denali fault zone (KLD 94) farthest to the southeast. In this area, the catchments mostly comprise magmatic rocks of the Coast Plutonic Complex (Fig. 3). Those samples show narrow distributions with the largest ZFT and AFT age components at ca. 70–45 Ma (Fig. 3, Table 2), which indicate relatively rapid cooling of these magmatic rocks following intrusion.

Due to the road that needed to be accessed to collect these samples, the catchments in the southeastern portion of the Eastern Denali fault are located northeast of the fault (except for KLD 95), while the catchments on the northwestern portion of the Eastern Denali fault are all located southwest of the fault (Fig. 3). Catchments in the Insular superterrane southwest of the Eastern Denali fault comprise basement and Late Jurassic–Early Cretaceous flysch of the Dezadeash Formation intruded by rocks of the ca. 120–105 Ma Chisana Arc, latest Eocene–Oligocene Amphitheatre clastics and Wrangell volcanic rocks (ca. 30–12 Ma in the study area). All of those catchments (KLD 109, KLD 103, KLD 104, and KLD 89) reveal Late Jurassic–Early Cretaceous AFT and ZFT age components with AFT age components being slightly younger than ZFT age components (Table 2, Fig. 3). These age components are not observed in samples from the Intermontane superterrane north of the Eastern Denali fault (KLD 3, KLD 1, KLD 38, KLD 92, KLD 93, KLD 96, and KLD 97; Fig. 3). Those catchments comprise basement rocks, a large portion of Dezadeash sediments, and intrusions of the ca. 85–45 Ma Kluane Arc (Fig. 3). All catchments both northeast and southwest of the Eastern Denali fault reveal AFT and ZFT age components ranging from 80 Ma to 30 Ma, which suggests that dominant cooling occurred during the Late Cretaceous–Oligocene (blue and green color in pie charts of Fig. 3, Table 2) on both sides of the Eastern Denali fault. Miocene and younger (<23 Ma) age populations are sparse in both detrital AFT and ZFT data and are generally small (<10% of all measured grains). These age components occur mostly in catchments southwest of the Eastern Denali fault (KLD 109, KLD 103, KLD 104, KLD 89, and KLD 95) but also in some catchments north of the fault (KLD 93 and KLD 97).

In summary, detrital data from catchments along the Eastern Denali fault recorded dominant Late Cretaceous–Oligocene cooling that occurred on both sides of the fault. Additionally, dominant Late Jurassic–Early Cretaceous cooling is observed in catchments composed by the Insular superterrane rock southwest of the Eastern Denali fault and the overlying Dezadeash sediments that are exposed along the fault (green unit in Fig. 3A).

Detrital AFT and ZFT Cooling Record between Eastern Denali and Fairweather Faults

The region between the Eastern Denali fault and the Fairweather fault is characterized by mountainous topography and large glacial systems of the Fairweather and Alsek ranges of the St. Elias Mountains (Figs. 1–2). To visualize the topography of this area, we present two 15-km-wide, SW–NE swath profiles that stretch from the Pacific Ocean across the Fairweather fault and Eastern Denali fault (Figs. 4A–4B) and one 20-km-wide, NW–SE profile that stretches parallel to the faults (Fig. 4C; location of swaths in Fig. 1). The Alsek River is the main drainage system in the area, and its catchment comprises numerous large glaciers (Figs. 2 and 5A). The headwater of the Alsek River reaches far north of the Eastern Denali fault, where it is characterized by lower topographic relief (Yukon plateau) than the region southwest of the Eastern Denali fault (Figs. 5A–5B). The Tatshenshini River is the largest tributary and composes the southeastern portion of the Alsek catchment (Fig. 2). The headwaters of the Tatshenshini River are northeast and southwest of the Eastern

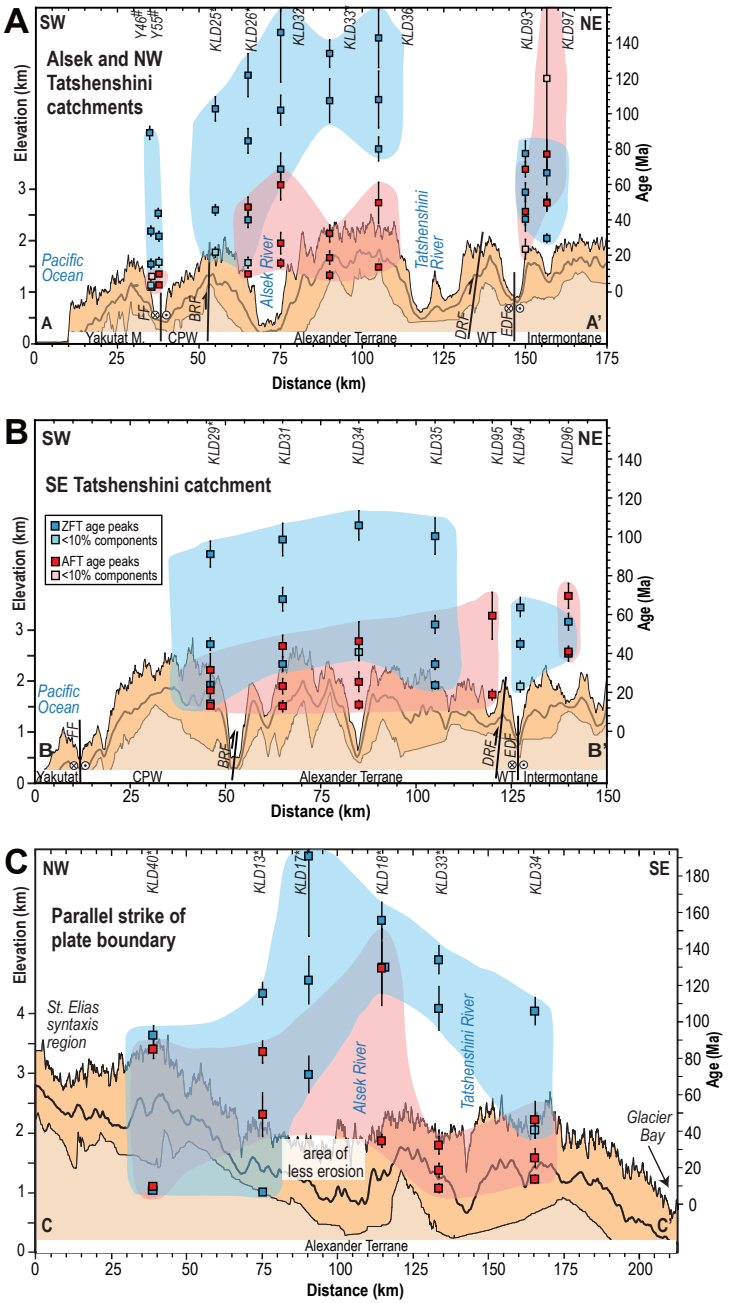

Figure 4. Swath profiles display the mean, maximum, and minimum elevations across (A–B) the Fairweather–Eastern Denali fault corridor and (C) along the strike of the corridor. Locations of swaths are indicated in Figures 1–2. Overlaid are apatite fission track (AFT) and zircon fission track (ZFT) age component peaks and 1σ errors from this study and published data. Data from Falkowski and Enkelmann (2016) are marked with *; AFT data from Enkelmann et al. (2015a) and ZFT data from Falkowski et al. (2014) are marked with #. FF—Fairweather fault, BRF—Border Ranges fault, DRF—Duke River fault, EDF—Eastern Denali fault, Yakutat M. and Yakutat—Yakutat microplate, CPW—Chugach-Prince William terrane, WT—Wrangellia terrane, Intermontane—Intermontane superterrane.

Denali fault and the Duke River fault, whereby the lower river cuts through the partially glaciated mountains that are underlain by the Insular superterrane (Figs. 5C–5D). The Tatshenshini–Alsek confluence is 12 km west of the Border Ranges fault and 55 km from the Pacific Ocean.

We present our new and published data as pie charts, histograms, and probability density plots with the peak fitting results for the Alsek River (Fig. 6) and the Tatshenshini River catchments (Fig. 7). Note that all published data are marked with an asterisk on their sample ID in figures and text. We also plot the component peak ages and 1σ errors of samples with catchments crossing the three swath profiles to show the data with respect to the topography (in Fig. 4, blue- and red-shaded areas outline the general trend of detrital age components). Emphasis is given to the youngest age components, as they record the most recent cooling that occurred in the catchments. In contrast, the older age components represent the crustal section that cooled slowly over longer times due to magmatic relaxation or slow erosion. The total widths of the age components in a catchment provide information about the amount of cooling and/or exhumation that occurred in a certain time interval. Overall, the spatial trend in the detrital age component peaks plotted along the two transects that cross the Fairweather and Eastern Denali faults shows an increase in peak ages and spread in age components with increasing distance from the plate boundary and an abrupt change in cooling ages across the Eastern Denali fault (Figs. 4A–4B). AFT age populations of <20 Ma occur across the entire Fairweather–Eastern Denali fault corridor but increase to >40 Ma northeast of the Eastern Denali fault (Figs. 4A–4B). ZFT ages are generally older (Early Cretaceous–Paleocene) than the AFT age peaks and increase with distance from the Fairweather fault but jump to younger ages (30–80 Ma) northeast of the Eastern Denali fault. Between profile A and B there is a distinct difference in the range of ZFT age components located between the Fairweather fault and the Eastern Denali fault. In profile A, ZFT age components increase inboard, and several of the samples show age peaks ranging from 60 Ma to >140 Ma. In contrast, in profile B, the ZFT age components show a smaller increase and no change with increasing distance from the plate boundary, and age components are generally younger and range from 40 Ma to 110 Ma (Fig. 4B). Only some of these spatial differences can be explained by the underlying bedrock geology within the various catchments. For example, there are much younger $^{40}Ar/^{39}Ar$ cooling ages (31–25 Ma) reported from Oligocene intrusions exposed in catchment KLD 35 (Fig. 5D). But otherwise, the underlying geologic units

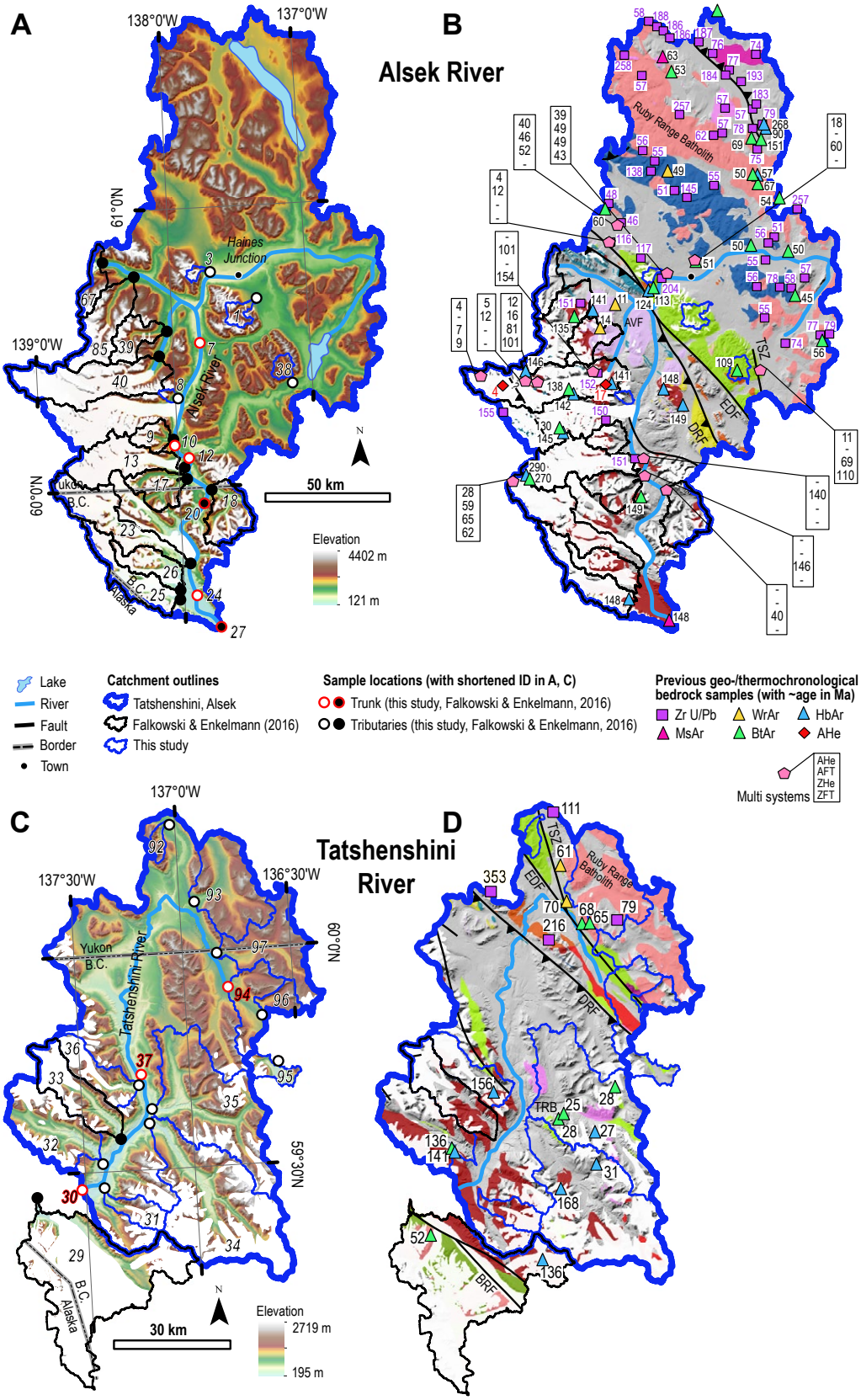

Figure 5. Topographic (based on ASTER GDEM V3 data) and geologic maps (A–B) are shown for areas on top of hillshades of the Alsek River catchment and (C–D) the Tatshenshini River catchment. Geology is from Yukon Geological Survey (Bedrock Geology Data set, http://data.geology.gov.yk.ca/Compilation/3#InfoTab, downloaded April 2019), and British Columbia Geological Survey (Cui et al., 2017). Black numbers are published geochronologic and thermochronologic ages in time increments of million years. Geochronology and high-temperature thermochronology data are from Hudson et al. (1977), Dodds and Campbell (1988), and Breitsprecher and Mortensen (2004; Yukon Geological Survey geochronology database, including updates until 2018, http://data.geology.gov.yk.ca/Compilation/22#InfoTab). Low-temperature thermochronology data are from Spotila and Berger (2010), Falkowski and Enkelmann (2016), Enkelmann et al. (2017), and McDermott et al. (2019). Zr U/Pb—zircon U/Pb; MsAr—muscovite K-Ar; WrAr—whole rock K-Ar; Bt—biotite K-Ar; HbAr—hornblende K-Ar, AHe; ZHe—apatite and zircon (U-Th)/He, respectively. B.C.—British Columbia, TSZ—Tatshenshini Shear Zone, EDF—Eastern Denali fault, DRF—Duke River fault, AVF—Alsek Volcanic Field, TRB—Tkope River Batholith (not represented in geologic map; Dodds and Campbell, 1988), BRF—Border Ranges fault.

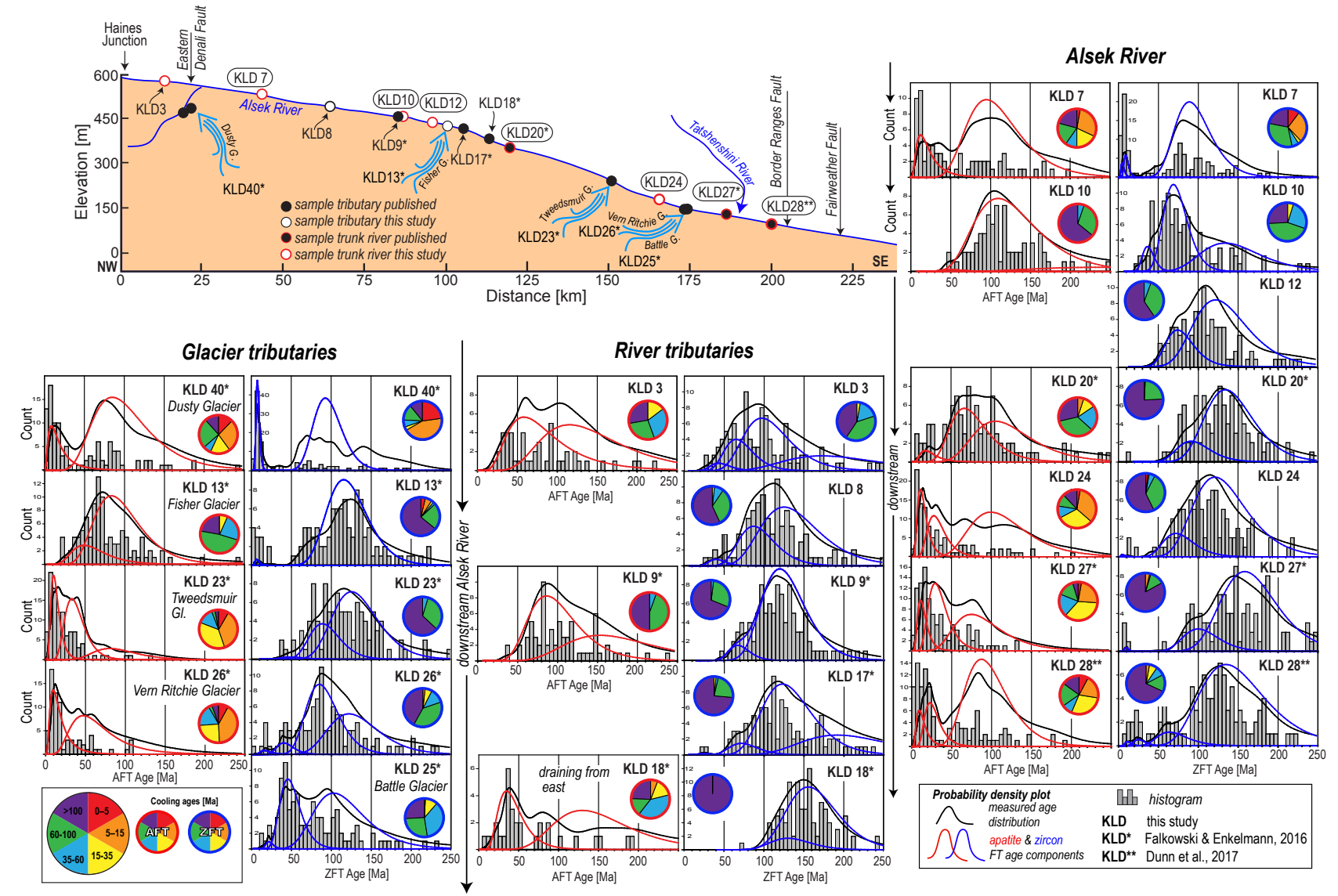

Figure 6. Alsek River profile indicates sample locations of the trunk river and tributaries. Histograms, probability density plots, and age component fitting curves (from Binomfit, Brandon, 1992, 1996) of detrital apatite fission track (AFT) and zircon fission track (ZFT) data are shown with pie charts representing single-grain ages. All vertical axes are probability. G.—Glacier.

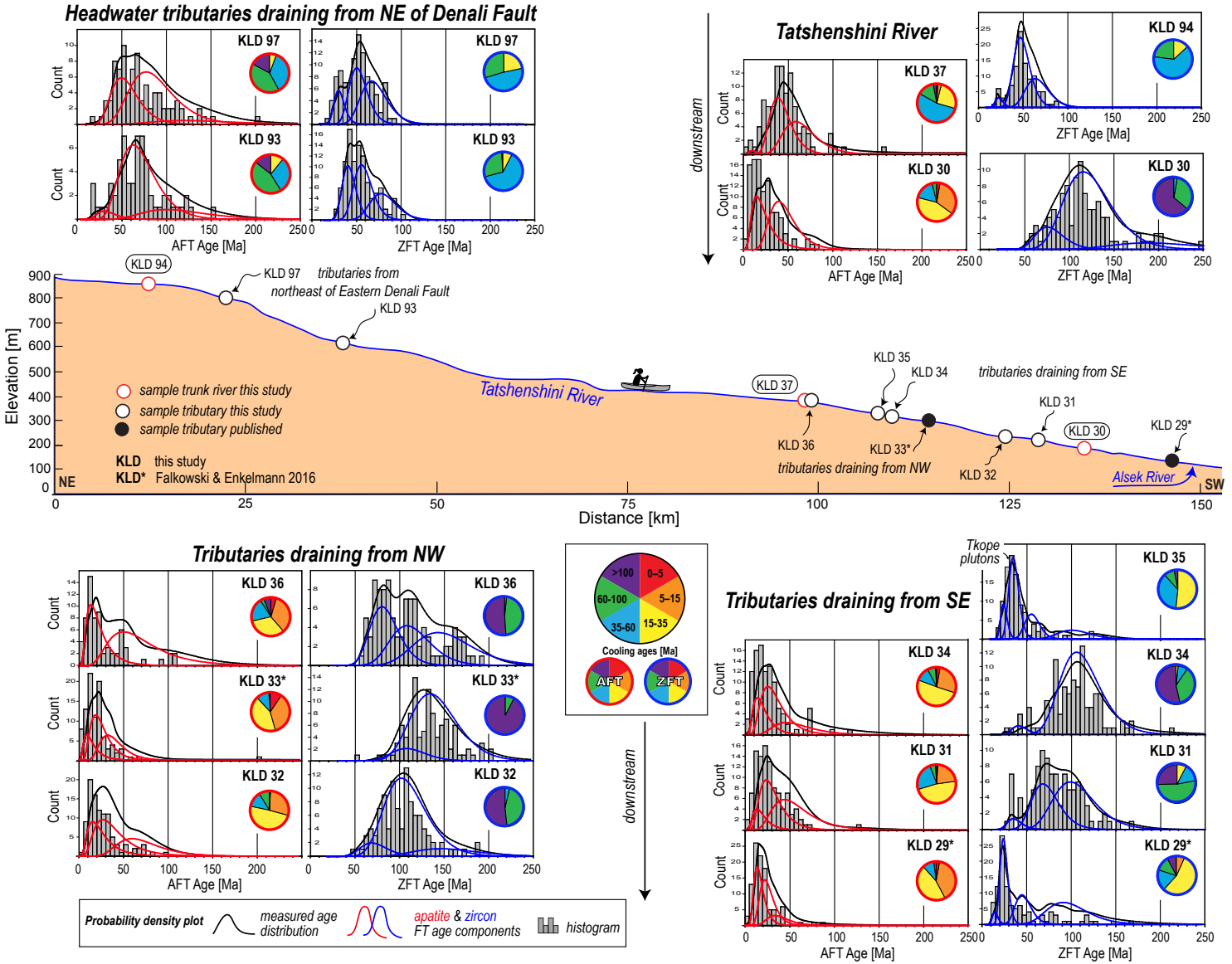

Figure 7. Tatshenshini River profile indicates sample locations of the trunk river and tributaries. Histograms, probability density plots, and age component fitting curves (from Binomfit, Brandon, 1992, 1996) of detrital apatite and zircon fission track (AFT and ZFT, respectively) data are shown with pie charts representing single-grain ages.

in the catchments of profiles A and B are similar. Bedrock geochronology reported from other catchments along swath profile B (e.g., KLD 31, KLD 34, and KLD 36) report ages similar (168–136 Ma) to those reported from bedrock exposed in catchments along profile A (e.g., KLD 25*, KLD 26*, KLD 32, and KLD 33*) (Figs. 5B and 5D). This suggests differences in upper crustal rock cooling and exhumation along the strike of the Fairweather and Eastern Denali fault corridor. The age component peaks plotted in the along-strike profile reveal those large changes (Fig. 4C). There are younger AFT and ZFT ages at the northwestern and southeastern end of the profile and older ages in the middle, where the profile line crosses the Alsek River.

Alsek River Catchment

We report four new samples collected from the Alsek River, of which three (KLD 7, KLD 10, and KLD 24) yielded AFT and ZFT data, while sample KLD 12 yielded ZFT data only (Fig. 6). AFT and ZFT data from three Alsek River samples were published previously (KLD 20* and KLD 27* by Falkowski and Enkelmann (2016) and KLD 28* by Dunn et al. (2017)). Ten tributary samples were analyzed, of which two are new (KLD 3 and KLD 8), and eight samples (KLD 9*, KLD 13*, KLD 17*, KLD 18*, KLD 23*, KLD 25*, KLD 26*, and KLD 40*) were reported by Falkowski and Enkelmann (2016). All 10 samples yielded ZFT data, and seven yielded AFT data (Fig. 6).

The ZFT age distributions found in the Alsek River catchment show a very heterogeneous cooling pattern. In general, most samples are dominated by ZFT grains >100 Ma (purple in pie charts in Fig. 6). The largest ZFT components peak in the Late Jurassic–Early Cretaceous between 160 Ma and 110 Ma and often comprise 50–90% of the samples' grains. Another large portion of the grains yielded ZFT dates between 100 Ma and 60 Ma (green in pie charts in Fig. 6) that correspond to the Late Cretaceous age component peaks that comprise mostly 30–50% of the sample (100–69 Ma; Tables 2 and S1 (footnote 1). In contrast, ZFT data derived from the Dusty Glacier catchment (KLD 40*) and nearby Alsek River sample (KLD 7) yielded much younger grains (red and orange in pie charts in Fig. 6). These young grains correspond to age component peaks of 7.6 ± 0.4 Ma (64%) in KLD 40* and 4.6 ± 0.7 (19%) and 9 ± 1 (21%) in KLD 7 (Tables 2 and S1). The AFT data reveal a larger variety in ages with dominantly young (35–0 Ma) grains in the large glacier tributaries (KLD 23*, KLD 26*, and KLD 40*) and in the Alsek River sediment further downstream. Dominant age components peak at 10.6 ± 0.8 Ma (60%) in KLD 23*, 9.4 ± 1.0 Ma (70%) in KLD 26*, and 8.8 ± 0.9 Ma (55%) in KLD 40*. Old AFT ages that are >60 Ma are found in small catchments draining from the east (KLD 9*) and the upper portion of the Alsek River (KLD 10). The dominant age components of these samples are 86.3 ± 6.2 Ma (71%) and 104.1 ± 6.3 Ma (61%), respectively. These old ages are similar to those obtained from catchments along the Eastern Denali fault (compare with data in Fig. 3). The distinctively young (<15 Ma) AFT and ZFT grains derived from the Dusty Glacier (KLD 40*) are thought to record exhumational cooling in the high icefield region based on bedrock cooling ages (Falkowski and Enkelmann, 2016). A similar young age signal is observed in sample KLD 7, which was collected just downstream of the Kaskawulsh-Alsek confluence and may record the Dusty Glacier signal and/or the erosion of local Miocene Wrangell volcanics (Fig. 5B). These locally exposed volcanics have been dated at 16–11 Ma (Stevens et al., 1982; Dodds and Campbell, 1988; Trop et al., 2012), which could explain the observed AFT age component (12.7 ± 1.4 Ma, 51%) but not the significant number of younger ZFT ages (component peaks at 4.6 ± 0.7 Ma (19%) and 9 ± 1 Ma (21%); Table 2). For that reason, we assume that this age signal is recording mostly the exhumational sediment signal of the Dusty Glacier. Farther downstream in the Alsek River (KLD 10 and KLD 12), the young age signal is entirely diluted by the sediment contribution of tributaries from the west and east (Figs. 5–6). The much smaller Fisher Glacier (KLD 13*) and all of the fluvial tributaries (KLD 8, KLD 9*, and KLD 17*) do not reach the syntaxis region and do not yield such young age components. Farther downstream, the Tweedsmuir (KLD 23*), Vern Ritchie (KLD 26*), and Battle (KLD 25*) Glaciers stretch far northwest into the St. Elias Mountains and parallel to the northern end of the Fairweather fault. KLD 23* and KLD 26* yield large (60–70%), late Miocene AFT age components (peaks at 10.6 ± 0.8 Ma and 9.4 ± 1.0 Ma) but few zircon grains that are that young (Figs. 5–6; Table S1 [footnote 1]). All three Alsek River samples collected below Tweedsmuir Glacier (KLD 24, KLD 27*, and KLD 28*) yield a dominant late Miocene (11–9 Ma; 31–51%) AFT age component, while ZFT age components of that age are very small (3–4%).

In summary, the detrital data from the Alsek River catchment reveals that most bedrock cooling below ca. 250 °C (ZFT system) occurred during the Jurassic and Cretaceous with the exception of the Dusty Glacier (KLD 40*) catchment, which shows significantly younger cooling (Fig. 6). Upper crustal cooling below ca. 110 °C (AFT system) also occurred during the Jurassic through Eocene time in the upper Alsek catchment and catchments located east of the river. This is in contrast to the cooling recorded by the detrital data from glacial tributaries located west of the Alsek River that reveal a downstream increase of the Miocene cooling record (Fig. 6).

Tatshenshini River Catchment

We present data from 12 samples collected within the Tatshenshini River catchment (Figs. 5C and 7), of which two have been published before (KLD 29* and KLD 33*; Falkowski and Enkelmann, 2016). Nine samples yielded AFT and ZFT data, while two samples yielded only ZFT data (KLD 94 and KLD 35), and one sample yielded only AFT data (KLD 37). When disregarding the smallest (<5%) age components, ZFT age components peak between 14.3 ± 1.5 Ma (9%) and 188 ± 22 Ma (7%), while AFT components peak from 8.7 ± 2.3 Ma (34%) to 77.2 ± 7.8 Ma (51%; Table 2). There is a clear difference in the data between the headwater tributaries located northeast of the Eastern Denali fault and tributaries further downstream the Tatshenshini River.

In the headwaters, ZFT single-grain ages mostly range between 60 Ma and 35 Ma (blue in pie charts; KLD 93, KLD 94, and KLD 97) with smaller portions of

younger (35–15 Ma, yellow) and older grains (100–60 Ma, green in pie charts; Fig. 7). The dominant ZFT age components are Late Cretaceous–Eocene (peak of 70–40 Ma; Table 2). The AFT single-grain age distributions show slightly older ages of Cretaceous–Eocene cooling that range from 100 Ma to 35 Ma (blue and green in pie charts, Fig. 7), and contain grains >100 Ma (purple, Fig. 7). However, the dominant AFT age components are similar to the ZFT data with Late Cretaceous to early Eocene peaks of 77–49 Ma (Table 2).

In the lower portion of the Tatshenshini River catchments, ZFT data are dominated by grains >60 Ma (green and purple in pie charts; KLD 30, KLD 32, KLD 33*, KLD 34, and KLD 36; Fig. 7). There are two exceptions to the relatively old ZFT data. One is sample KLD 35, which reveals large age components that peak at ca. 35 Ma (55%) and ca. 24 Ma (22%). This tributary catchment comprises Oligocene intrusive rocks that are most likely the source for these younger grains, and they thus do not record exhumational cooling (Fig. 5D; Tkope plutonic suite; Dodds and Campbell, 1988). The other exception is KLD 29*, which is a large glacial catchment that connects with the high ice-field region of the Mount Fairweather massif (>4000 m elevation) that characterizes the southern end of the Fairweather fault. This tributary glacier follows the Border Ranges fault, which separates the Insular superterrane from the Chugach-Prince William terrane (Figs. 1–2). The ZFT and AFT age distributions from that sample reveal large Miocene age components with peaks at 14–13 Ma and 24–21 Ma for both systems (Fig. 7; Table S1).

The AFT data of the Tatshenshini River catchment reveal that most grains cooled in the Oligocene to Miocene and are <35 Ma (red, orange, and yellow in pie charts; Fig. 7). All Tatshenshini tributaries reveal a dominant AFT age component that peaks at 18–9 Ma, which suggests that this region underwent exhumation since the mid Miocene (Tables 2 and S1 [footnote 1]). This is in contrast to AFT ages from the neighboring catchments (Alsek tributaries KLD 3, KLD 9*, and KLD 18*; Fig. 6) that show much older (>35 Ma and mostly >60 Ma) AFT ages and dominant age components that peak at 86–34 Ma (Tables 2 and S1).

In summary, the catchments in the headwaters of the Tatshenshini River, which are located northeast of the Eastern Denali fault, yielded similar Late Cretaceous–Eocene AFT and ZFT age components, which suggest cooling from >250 °C to below 110 °C at that time. Detrital data from tributary catchments draining into the lower Tatshenshini River record rapid Miocene cooling (>10 °C/m.y.; KLD 29*, KLD 31, KLD 32, KLD 33*, KLD 34, and KLD 36) from below the AFT closure temperature. Miocene deep-seated and rapid exhumation from below the ZFT closure depths occurred along the Border Ranges fault (KLD 29*).

DISCUSSION

We summarize the new and previous detrital data from our study area and the St. Elias Mountains to provide an orogen-scale perspective of the cooling record. Our new results, integrated with previous detrital data, cover a large region (~20,000 km^2) that is very remote and partially covered by extensive glaciers (Figs. 2–3). The detrital ZFT and AFT data provide an integrated cooling signal of rocks below ~250 °C and ~110 °C (e.g., Brandon et al., 1998; Ketcham et al., 1999), which we can largely relate to exhumation in the upper crust. We first discuss crustal cooling along and across the Eastern Denali fault (Fig. 3) and then the mountainous region between the Fairweather fault and the Eastern Denali fault. We specifically focus on the role of the Alsek and Tatshenshini Rivers in eroding material and driving rock exhumation (Figs. 4–8). Figure 8 shows the outline of catchments from which detrital AFT and/or ZFT are available from this and previous studies. Pie charts are shown for representative samples or combinations of samples to provide a visual summary of variations in age distributions over the broader region (Table S3 [see footnote 1]). The varied gray shading of the catchments is used to distinguish between sample(s) represented by one pie chart. If samples were combined, it was based on their similarity in age distribution and spatial proximity to reduce the number of charts shown. These data are compared with the downstream change of the detrital AFT and ZFT record from the Alsek and Tatshenshini Rivers (right side of Figs. 8A–8B).

Exhumation Record along the Eastern Denali Fault

The Denali fault is a continental-scale structure that stretches for more than 2000 km from northernmost British Columbia through southwestern Yukon and southcentral Alaska to the Bering Sea (Fig. 1). The onset and history of its activity is not certain, but initiation as a shear zone within the Intermontane and Insular collision zone was suggested for the Late Cretaceous (Lowey, 1998). The bulk of right-lateral displacement occurred after ca. 57 Ma and possibly with continuous slip until present (Eisbacher, 1976; Nokleberg et al., 1985; Lowey, 1998; Andronicos et al., 1999; Cole et al., 1999; Gehrels, 2000; Miller et al., 2002; Ridgway et al., 2002; Riccio et al., 2014; Haeussler et al., 2017).

Thermochronologic studies that investigate exhumation across and along the Eastern Denali fault are sparse; in total, only 15 bedrock samples have been analyzed from the area (Fig. 3; Spotila and Berger, 2010; Falkowski and Enkelmann, 2016; Enkelmann et al., 2017; McDermott et al., 2019). While the studies by Spotila and Berger (2010), Falkowski and Enkelmann (2016), and Enkelmann et al. (2017) focused on the regional exhumation pattern of the St. Elias Mountains, only the study by McDermott et al. (2019) specifically attempted to quantify exhumation across the Eastern Denali fault in the region of Kluane Lake. McDermott et al. (2019) suggested three exhumation phases including: (1) Late Cretaceous (95–75 Ma) rapid exhumation and high relief on both sides due to terrane accretion and Eastern Denali fault activity; (2) Late Cretaceous–Oligocene (75–30 Ma) slow exhumation of a stable, low-relief landscape southwest of the Eastern Denali fault due to a shift of deformation to the northeast of the Eastern Denali fault and/or pure strike-slip Eastern Denali fault activity; and (3) Oligocene–Present (30–0 Ma) rapid exhumation and surface uplift in a transpressional setting southwest of the Eastern Denali fault possibly caused by Yakutat microplate subduction and collision. No thermochronological data exist from the southeastern part of the Eastern Denali

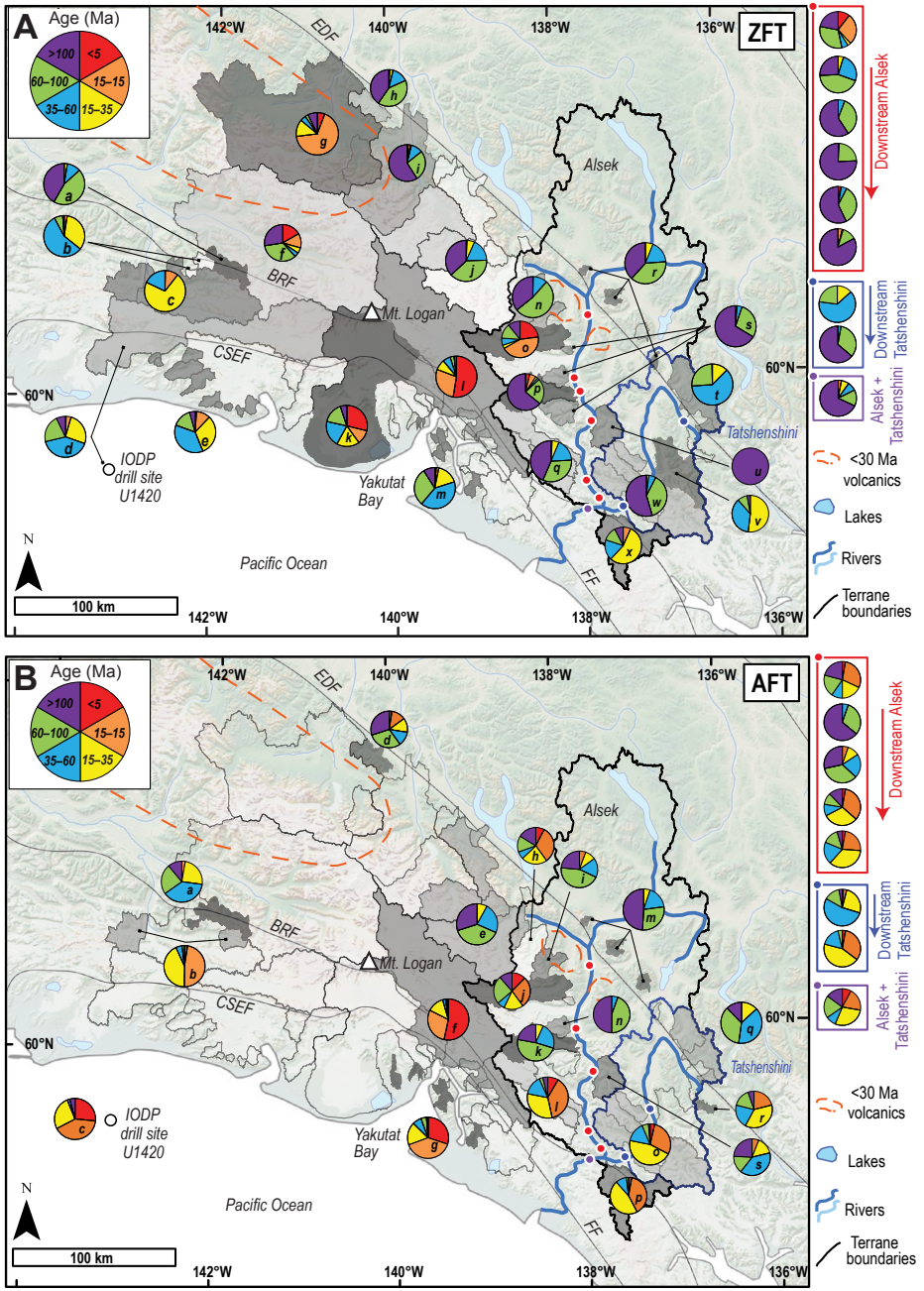

Figure 8. Compilation shows all new and published (A) detrital zircon and (B) apatite fission track data from the St. Elias Mountains and offshore. Pie charts are shown for representative samples (data were combined when neighboring catchments showed similar age distributions). Gray shading of catchments indicates for which catchment(s) pie charts are shown. See Table S3 (see footnote 1) for sample IDs and references (sorted by pie chart designations a–x for ZFT and a–s for AFT). Pie charts of samples collected from the Alsek and Tatshenshini trunk rivers are shown on the right side of the map. FF—Fairweather fault; EDF—Eastern Denali fault; BRF—Border Ranges fault; CSEF—Chugach-St. Elias fault; IODP—Integrated Ocean Drilling Program.

fault (Fig. 3), and thus our new detrital AFT and ZFT data from 14 catchments provide the first information on rock cooling along the majority of the length of the Eastern Denali fault and a wider corridor (Fig. 3).

Older detrital AFT and ZFT age components (ca. 170–85 Ma, Table 2) are preserved on both sides of the Eastern Denali fault. Catchments southwest of the Eastern Denali fault are underlain by Insular basement, Gravina sediments, and mid-Cretaceous magmatic rocks (Fig. 3). Northeast of the Eastern Denali fault, the older age components are restricted to the Gravina belt (green-colored Dezadeash Formation; Figs. 3A and 8A). In the Intermontane superterrane, older cooling signals were overprinted by the early Cenozoic intrusions and metamorphism in the study area. The ca. 170–85 Ma age components represent cooling associated with the time before and during collision of the Insular and Intermontane superterranes. That period includes volcanic arc activity (Chitina Arc at ca. 160–130 Ma, and Chisana Arc at 120–105 Ma; see Figs. 5B and 5D; Dodds and Campbell, 1988), which sourced the Dezadeash flysch (Berg et al., 1972; Eisbacher, 1976; Lowey, 1992), basin closure, deformation along the entire suture, and development of the Denali fault (e.g., Dusel-Bacon et al., 1993; Andronicos et al., 1999; Israel et al., 2014; McDermott et al., 2019). The tectonic setting was transpressional, and oblique plate convergence resulted in crustal thickening and exhumation in the entire North American Cordillera (e.g., Engebretson et al., 1985; Farmer et al., 1993). During this time, the Duke River fault was an active northeast-vergent thrust fault (muscovite $^{39}Ar/^{40}Ar$, 105–79 Ma; Cobbett et al., 2017).

Most of the detrital samples reveal Late Cretaceous–Oligocene AFT and ZFT age components (75–30 Ma; Table 2), which suggests that both sides of the Eastern Denali fault experienced crustal cooling at this time. We hypothesize that the two regions, located southwest and northeast of the Eastern Denali fault, were juxtaposed during their time of upper crustal cooling and displaced dextrally afterwards. This Late Cretaceous–Oligocene cooling phase coincides with cooling phase two of McDermott et al. (2019), for which they suggested slow cooling and decaying topography southwest of the Eastern Denali fault. The reason for this discrepancy between their suggested slow cooling and the more rapid cooling suggested by our data is probably caused by the limited spatial coverage of the bedrock studies in comparison to the detrital data (compare Fig. 3A with Figs. 3B and 8). This timing of cooling coincides with the activity of the Tatshenshini (TSZ in Fig. 2) and the Coast Shear zones (Ingram and Hutton, 1994; Lowey, 2000) and the suggested rapid unroofing of the Paleocene Kluane Arc rocks (55–39 Ma; Farrar et al., 1988; Israel et al., 2011), all of which are located northeast of the Eastern Denali fault. However, latest Eocene–Oligocene strike-slip basins developed southwest of the Eastern Denali fault (Amphitheatre Formation). The sediment deposited in these basins is sourced from both the Insular and Intermontane superterranes (Ridgway and DeCelles, 1993a). Based on our new data, we suggest that uplift and rock exhumation must have also occurred southwest of the Eastern Denali fault during Late Cretaceous–Oligocene time. This supports the suggested existence of high local relief at the time when the Amphitheatre Formation was deposited (Ridgway and DeCelles, 1993a, 1993b).

ZFT and AFT ages, and age components younger than 30 Ma, are generally sparse (yellow in pie charts of Figs. 3B and 8). Some catchments yielded AFT age components that make up >24% of the samples' grains and peak at ca. 29–11 Ma (KLD 109, KLD 102, KLD 97, and KLD 95; Fig. 3B, Table 2). These samples are located on both sides of the Eastern Denali fault. In general, <30 Ma cooling ages in southern Alaska, southwest Yukon, and northwestern British Columbia are interpreted to reflect Yakutat subduction and collision (red, orange, and yellow in pie charts of Fig. 8). Bedrock thermochronology yielded Miocene (<20 Ma) apatite (U-Th)/He and AFT cooling ages in the fault zone some distance (>5 km) northeast of the Eastern Denali fault (Enkelmann et al., 2017; McDermott et al., 2019). However, the youngest ages, including zircon (U-Th)/He ages, are from rocks located <2 km from the Eastern Denali fault (Fig. 3A; McDermott et al., 2019). McDermott et al. (2019) suggest ca. 30 Ma developments of higher topography and relief along the Eastern Denali fault and southwest of it with limited exhumation in the Intermontane superterrane. This suggestion is consistent with the detrital AFT and ZFT data that contain older age components (30–20 Ma) northeast of the Eastern Denali fault and younger age components (<20 Ma) southwest of the Eastern Denali fault (Fig. 4). This age pattern suggests that earlier exhumation occurred northeast of the Eastern Denali fault, which later must have shifted southwest of the fault. This interpretation also agrees with a recent geophysical study that investigated the 2017 earthquake couplet and aftershocks along the southern end of the Eastern Denali fault (yellow star in Fig. 2). The seismic data suggest that today the southern end of the Eastern Denali fault acts as a deformational backstop that focuses distributed rock strain in the region between the Fairweather plate boundary and the Eastern Denali fault (Choi et al., 2021).

Exhumation between the Fairweather Fault and the Eastern Denali Fault

Previous studies argued that the Yakutat collision resulted in Miocene and younger deformation and rock exhumation within only <30 km northeast of the plate boundary in the area of the St. Elias syntaxis (Enkelmann et al., 2017). Miocene and younger exhumation appears to reach farther inboard from the plate boundary south of the syntaxis region and along the northern end of the Fairweather fault (Fig. 8) (Enkelmann et al., 2017). Bedrock studies along the Fairweather fault document exhumation since ca. 5 Ma in a 10 km narrow zone along the fault (O'Sullivan et al., 1997; McAleer et al., 2009). In the Yakutat Bay area, bedrock and detrital thermochronology reveal exhumation that began at ca. 30 Ma and 10–12 km of exhumation that has occurred since at least 3 Ma between the Fairweather fault and the nearby Border Ranges fault (Fig. 8; Falkowski et al., 2014; Enkelmann et al., 2015a, 2015b; Schartman et al., 2019). Further south along the Fairweather fault, in the lower Alsek River valley, bedrock apatite FT and (U-Th)/He ages are <3 Ma, and zircon (U-Th)/He ages are 17–13 Ma, which suggests cooling since mid-Miocene time that accelerated at ca. 5 Ma (O'Sullivan et al., 1997; McAleer et al., 2009). Rapid advection and rock exhumation occur southwest of the plate boundary at the

restraining bend located at the southern end of the Fairweather fault (Lease et al., 2021). This study suggests that the rocks northeast of the plate boundary act as a backstop for deformation. However, only apatite (U-Th)/He data are available from this area, which all suggest that cooling below 60 °C occurred at 3–1 Ma (Lease et al., 2021). Similar young apatite (U-Th)/He ages are reported from Glacier Bay, which is located more inboard at the southernmost end of the Fairweather fault and records cooling at 8–2 Ma (McAleer et al., 2009).

Our detrital data provide a first order cooling and exhumation signal from farther inboard of the Fairweather fault (Fig. 8), where bedrock thermochronology data are missing. Unlike the pattern inboard from the syntaxis region, the entire corridor between the Fairweather and the Eastern Denali fault reveals that the youngest AFT age components (P1 in Table 2 and Table S1 [footnote 1]) have peaks of <20 Ma and comprise 23%–70% of the measured grains (Figs. 4A–4B). This suggests that Miocene exhumation reached ca. 100 km inboard of the Fairweather plate boundary. There is a distinct change in AFT data to age components that peak at >40 Ma northeast of the Eastern Denali fault. ZFT ages are generally old southwest of the Eastern Denali fault but are distinctively younger (80–30 Ma) to its northeast (Figs. 4A–4B). This pattern suggests that the Insular and Intermontane superterranes record different exhumation histories. The old ZFT data suggest that the Insular superterrane rocks exhumed only modestly to less than 10 km as the Yakutat microplate moved northwestward along the highly oblique North American plate boundary. The Intermontane superterrane records significant exhumation in the Late Cretaceous–Eocene (e.g., Eisbacher, 1976; Nokleberg et al., 1985; Riccio et al., 2014) followed by very little exhumation (<4 km) since 30 Ma. The lack of Miocene and younger age components across the Eastern Denali fault suggests that the Intermontane superterrane may have served as a backstop for more recent exhumation. No detailed structural mapping has been conducted in this remote region that would allow evaluating if Miocene exhumation of the Insular superterrane was driven by deformation. However, there is some evidence for faulting. Bedrock apatite (U-Th)/He and ZFT data collected from west and east across the Dusty Glacier valley jump from 4.3 Ma to 16.6 Ma and 9.4–101 Ma, respectively (Falkowski and Enkelmann, 2016). This sudden change in ages suggests a possible fault underneath the ice that runs parallel to the Duke River fault. Cobbett et al. (2017) investigated the structural relationships along the Duke River fault and suggest that post-Miocene thrusting over Wrangell volcanic rocks occurred in the upper Tatshenshini River catchment region. This suggestion of compressional deformation agrees with the current deformation pattern revealed by the seismic record. Compressional dip-slip and strike-slip deformation is widely distributed between the plate boundary and the Eastern Denali fault and does not appear to be focused along a specific structure such as the Eastern Denali fault or the Duke River fault (Doser and Rodriguez, 2011). The seismicity is very sparse northeast of the Eastern Denali fault. Investigations of the 1 May 2017 earthquake couplet and more than 3000 aftershocks suggest that the Eastern Denali fault acts as a backstop for current deformation (Choi et al., 2021). The calculated maximum stresses are oriented perpendicular to the strike of the Eastern Denali fault, which makes the fault unlikely to experience reactivated dextral slip (Choi et al., 2021).

Differential Exhumation along the Strike of the Plate Boundary

Our data reveal differences in rock cooling and exhumation along the strike of the Fairweather–Eastern Denali fault corridor (Fig. 4). The youngest age components occur at the northwestern and southeastern ends of the along-strike profile, and older ages occur in the middle, where the profile line crosses the Alsek River (Fig. 4C). This trend inversely mimics the topography (Fig. 4C). In the area of the middle Alsek River, where it cuts the profile line, the mean elevation is lowest ~1 km), and the AFT and ZFT age components are older. In contrast, the area further northwest and southeast has mean elevations of >1 km and age components are younger (Fig. 4C). The younging toward the heavily glaciated St. Elias syntaxis is expected. Previous detrital and bedrock thermochronology studies documented that extremely rapid (>5 km/m.y.) and deep-seated exhumation (ZFT age components of 2 Ma) occurred underneath the Kluane icefield, which is surrounded by the highest peaks of the orogen (i.e., Mt. Logan and Mt. St. Elias) (red and orange in ZFT pie chart l and AFT pie chart f in Fig. 8) (e.g., Enkelmann et al., 2009; Spotila and Berger, 2010; Falkowski and Enkelmann, 2016; Enkelmann et al., 2017). However, the younging of the P1 age components within the catchments of the lower Tatshenshini River is unexpected (compare AFT pie o with pie k, n, and s in Fig. 8B). The implication of this pattern is that rocks in the Tatshenshini River catchment experienced more recent exhumation from 110 °C depths than rocks in the middle portion of the Alsek River catchment (between Lowell and Tweedsmuir Glaciers), where the river is characterized by narrow canyons (marked region in Fig. 4C, ZFT pie charts s and u in Fig. 8A and AFT pie charts n and s in Fig. 8B). This region of less rock cooling and exhumation around the middle section of the Alsek River is also seen in the downstream change of ZFT and AFT data from the Alsek trunk river samples that show a change from young cooling ages to older cooling ages in the middle section of the river before changing to young ages in the lower Alsek River (right side of Fig. 8).

One possible explanation for the spatial pattern in the detrital data is that the Tatshenshini drainage is older and was the main drainage that eroded and transported material into the Gulf of Alaska. The young AFT and ZFT grains and age components found in the Dusty Glacier sample (KLD 40*) and the upper Alsek River sample (KLD 7; Figs. 6 and 8) require an effective evacuation system for the eroded material from the upper Alsek drainage over time (Falkowski and Enkelmann, 2016). We therefore hypothesize that the upper Alsek River was part of the ancestral Tatshenshini drainage that flowed farther southeast around the region of lower erosion in the middle Alsek River catchment. In this scenario, the Alsek River must have been much shorter and captured its northern drainage more recently. More research is needed to link the millennial-scale evolution of the Alsek River with the long-term exhumational pattern of this region.

On a larger scale, extending the along-strike profile (Fig. 4C) toward the northwest, the thermochronologic ages become much older. All glacial catchments that drain toward the north, which is part of the Yukon drainage network, yield dominantly AFT and ZFT single-grain dates of >60 Ma (Fig. 8) and age

components that peak at >50 Ma (Falkowski and Enkelmann, 2016). Bedrock ages reported from north of the St. Elias syntaxis region also report that apatite (U-Th)/He and AFT ages are >50 Ma (Spotila and Berger, 2010; Enkelmann et al., 2017). These studies suggest that exhumation driven by the Yakutat collision reaches <30 km inboard of the plate boundary, which contrasts with the 100-km-wide corridor of exhumation observed in the Fairweather-Eastern Denali fault corridor. It is unclear if the transition between these two regions is gradual or rather abrupt. This large-scale change in exhumation pattern also correlates with a change in seismicity. While the Fairweather-Eastern Denali fault corridor is characterized by a widely distributed seismic record (Doser and Rodriguez, 2011), the region farther to the northwest is characterized by fewer events that coincide spatially with the Totschunda, Duke River, and Connector faults (Doser, 2014). It thus appears that the crust inboard of the Yakutat indenter corner deforms differently, which seems to be reflected in the long-term exhumation record.

Timing of Exhumation between the Fairweather Fault and the Eastern Denali Fault

The dominant age components found in catchments located between the Fairweather fault and the Eastern Denali fault, excluding the catchments of the middle Alsek River (KLD 8, KLD 9*, KLD 13*, and KLD 17*), peak at 18–10 Ma, which suggests that this region underwent exhumation since the mid Miocene. This exhumation signal coincides with the suggested increase in exhumation within the St. Elias syntaxis region involving rocks of both the North American plate and the indenting Yakutat microplate (Grabowski et al., 2013; Falkowski et al., 2014, 2016; Enkelmann et al., 2017). We suggest that the recorded cooling since the mid Miocene in the Fairweather–Eastern Denali fault corridor records exhumation that was possibly driven by the oblique convergence of the Yakutat microplate. The only evidence for deformation at this time comes from the Duke River fault, which shows thrusting over Miocene Wrangell volcanics (Cobbett et al., 2017). Thus, we can only speculate about whether the Yakutat transport along the plate boundary caused deformation that drove exhumation within the entire Fairweather-Eastern Denali fault corridor. Alternatively, exhumation may have been driven by isostatic uplift of the entire crustal block that was thickened by previous plate convergence. The young rock exhumation reaches ca. 100 km inboard of the strike-slip–dominated plate boundary and thus much farther inboard than in the syntaxial region and west of it, where the plate boundary is characterized by convergence (Fig. 8). No Pliocene or younger cooling ages are found in our study area, which suggests moderate rock exhumation rates (<0.4 km/m.y.) since the mid Miocene. The Pliocene–Pleistocene glaciation of the St. Elias Mountains is suggested to have increased erosion and rock exhumation, but our data do not record such a change because exhumation did not exceed ca. 4 km since that time. Lower temperature studies such as apatite (U-Th)/He (closure temperature of 65–55 °C) would be needed to record this latest erosional phase.

CONCLUSIONS

Based on our new detrital AFT and ZFT data from 27 catchments integrated with previously published bedrock and detrital data, we show that significant cooling and rock exhumation occurred in the Intermontane and the Insular superterrane rocks in our study area during Late Cretaceous–Eocene time. Yakutat collision resulted in exhumation starting in the mid Miocene and occurred across the ca. 100-km-wide corridor between the Fairweather transform plate boundary and the Eastern Denali fault. Exhumation appears to be distributed across the entire crustal block and not localized along the Fairweather and Eastern Denali faults. This pattern contrasts significantly with the <30 km inboard reach of deformation and exhumation from the plate boundary in the St. Elias syntaxial corner. Despite the more convergent plate motion, exhumation inboard of the indenting plate corner is very limited. The Intermontane superterrane located northeast of the Eastern Denali fault acts as a backstop and has experienced minimal rock exhumation since the early Miocene.

ACKNOWLEDGMENTS

This study was funded by the Deutsche Forschungsgemeinschaft (DFG grants EN-941/1 and EN-941/1–2 to E. Enkelmann) and the Natural Sciences and Engineering Research Council of Canada (Discovery Grant RGPIN-2018–03932 and Northern Region Supplement NRS-2018-517959 to E. Enkelmann). We thank reviewers P. Armstrong, A. Meigs, and J. Spotila and associate editor J. Lee for constructive comments that improved the manuscript. All new data presented in this manuscript are archived at www.geochron.org.

REFERENCES CITED

Andronicos, C.L., Hollister, L.S., Davidson, C., and Chardon, D., 1999, Kinematics and tectonic significance of transpressive structures within the Coast Plutonic Complex, British Columbia: Journal of Structural Geology, v. 21, p. 229–243, https://doi.org/10.1016/S0191-8141(98)00117-5.

Arkle, J.C., Armstrong, P.A., Haeussler, P.J., Prior, M.G., Hartman, S., Sendziak, K.L., and Brush, J.A., 2013, Focused exhumation in the syntaxis of the western Chugach Mountains and Prince William Sound, Alaska: Geological Society of America Bulletin, v. 125, p. 776–793, https://doi.org/10.1130/B30738.1.

Armstrong, R.L., 1988, Mesozoic and early Cenozoic magmatic evolution of the Canadian Cordillera, *in* Clark, Jr., S.P., Burchfiel, B.C., and Suppe, J., eds., Processes in Continental Lithospheric Deformation: Geological Society of America Special Paper 218, p. 55–92, https://doi.org/10.1130/SPE218-p55.

Bemis, S.P., Weldon, R.J., and Carver, G.A., 2015, Slip partitioning along a continuously curved fault: Quaternary geologic controls on Denali fault system slip partitioning, growth of the Alaska Range, and the tectonics of south-central Alaska: Lithosphere, v. 7, no. 3, p. 235–246, https://doi.org/10.1130/L352.1.

Benowitz, J.A., Layer, P.W., Armstrong, P., Perry, S.E., Haeussler, P.J., Fitzgerald, P.G., and Van Laningham, S., 2011, Spatial variations in focused exhumation along a continental-scale strike-slip fault: The Denali fault of the eastern Alaska Range: Geosphere, v. 7, p. 455–467, https://doi.org/10.1130/GES00589.1.

Berg, H.C., Jones, D.L., and Richter, D.H., 1972, Gravina–Nutzotin belt—tectonic significance of an Upper Mesozoic sedimentary and volcanic sequence in southern and southeastern Alaska: U.S. Geological Survey Professional Paper 800D, p. D1–D24.

Berger, A.L., Spotila, J.A., Chapman, J.B., Pavlis, T.L., Enkelmann, E., Ruppert, N.A., and Buscher, J.T., 2008, Architecture, kinematics, and exhumation of a convergent orogenic wedge: A thermochronological investigation of tectonic-climatic interactions within the central St. Elias orogen, Alaska: Earth and Planetary Science Letters, v. 270, p. 13–24, https://doi.org/10.1016/j.epsl.2008.02.034.

Berkelhammer, S.E., Brueseke, M.E., Benowitz, J.A., Trop, J.M., Davis, K., Layer, P.W., and Weber, M., 2019, Geochemical and geochronological records of tectonic changes along a flat-slab arc-transform junction: Circa 30 Ma to ca. 19 Ma Sonya Creek volcanic field, Wrangell Arc, Alaska: Geosphere, v. 15, p. 1508–1538, https://doi.org/10.1130/GES02114.1.

Brandon, M.T., 1992, Decomposition of fission-track grain-age distributions: American Journal of Science, v. 292, no. 8, p. 535–564, https://doi.org/10.2475/ajs.292.8.535.

Brandon, M.T., 1996, Probability density plot for fission-track grain-age samples: Radiation Measurements, v. 26, p. 663–676, https://doi.org/10.1016/S1350-4487(97)82880-6.

Brandon, M.T., Roden-Tice, M.K., and Garver, J.I., 1998, Late Cenozoic exhumation of the Cascadia accretionary wedge in the Olympic Mountains, Northwest Washington State: Geological Society of America Bulletin, v. 110, p. 985–1009, https://doi.org/10.1130/0016-7606(1998)110<0985:LCEOTC>2.3.CO;2.

Breitsprecher, K., and Mortensen, J.K., 2004, Yukonage 2004: A database of isotopic age determinations for rock units from Yukon territory, Canada: Whitehorse, Yukon, Canada, Yukon Geological Survey, CD-ROM.

Brennan, P.K., and Ridgway, K.D., 2015, Detrital zircon record of Neogene exhumation of the central Alaska Range: A far-field upper plate response to flat-slab subduction: Geological Society of America Bulletin, v. 127, p. 945–961, https://doi.org/10.1130/B31164.1.

Brothers, D.S., Elliott, J.L., Conrad, J.E., Haeussler, P.J., and Kluesner, J.W., 2018, Strain partitioning in southeastern Alaska: Is the Chatham Strait Fault active?: Earth and Planetary Science Letters, v. 481, p. 362–371, https://doi.org/10.1016/j.epsl.2017.10.017.

Brueseke, M.E., Benowitz, J.A., Trop, J.M., Davis, K.N., Berkelhammer, S.E., Layer, P.W., and Morter, B.K., 2019, The Alaska Wrangell Arc: ~30 Ma of subduction-related magmatism along a still active arc-transform junction: Terra Nova, v. 31, p. 59–66, https://doi.org/10.1111/ter.12369.

Bruhn, R.L., Pavlis, T.L., Plafker, G., and Serpa, L., 2004, Deformation during terrane accretion in the Saint Elias orogen, Alaska: Geological Society of America Bulletin, v. 116, p. 771–787, https://doi.org/10.1130/B25182.1.

Bruhn, R.L., Sauber, J., Cotton, M.M., Pavlis, T.L., Burgess, E., Ruppert N., and Forster, R.R., 2012, Plate margin deformation and active tectonics along the northern edge of the Yakutat Terrane in the Saint Elias Orogen, Alaska, and Yukon, Canada: Geosphere, v. 8, p. 1384–1407, https://doi.org/10.1130/GES00807.1.

Chapman, J.B., Pavlis, T.L., Bruhn, R.L., Worthington, L.L., Gulick, S.P., and Berger, A.L., 2012, Structural relationships in the eastern syntaxis of the St. Elias orogen, Alaska: Geosphere, v. 8, p. 105–126, https://doi.org/10.1130/GES00677.1.

Choi, M., Eaton, D.W., and Enkelmann, E., 2021, Is the Eastern Denali fault still active?: Geology, v. 49, p. 662–666, https://doi.org/10.1130/G48461.1.

Cobbett, R., Israel, S., Mortensen, J., Joyce, N., and Crowley, J., 2017, Structure and kinematic evolution of the Duke River fault, Southwestern Yukon: Canadian Journal of Earth Sciences, v. 54, p. 322–344, https://doi.org/10.1139/cjes-2016-0074.

Cole, R.B., Ridgway, K.D., Layer, P.W., and Drake, J., 1999, Kinematics of basin development during the transition from terrane accretion to strike-slip tectonics. Late Cretaceous-early Tertiary Cantwell Formation, south central Alaska: Tectonics, v. 18, p. 1224–1244, https://doi.org/10.1029/1999TC900033.

Coney, P.J., Jones, D.L., and Monger, J.W., 1980, Cordilleran suspect terranes: Nature, v. 288, p. 329–333, https://doi.org/10.1038/288329a0.

Cui, Y., Miller, D., Schiarizza, P., and Diakow, L.J., 2017, British Columbia digital geology: British Columbia Geological Survey Open File 2017-8, 9 p.

Dodds, C.J., and Campbell, R.B., 1988, Potassium-argon ages of mainly intrusive rocks in the Saint Elias Mountains, Yukon and British Columbia: Geological Survey of Canada Paper 87-16, 43 p., https://doi.org/10.4095/126100.

Doser, D.I., 2014, Seismicity of Southwestern Yukon, Canada, and its relation to slip transfer between the Fairweather and Denali fault systems: Tectonophysics, v. 611, p. 121–129, https://doi.org/10.1016/j.tecto.2013.11.018.

Doser, D.I., and Rodriguez, H., 2011, A seismotectonic study of the Southeastern Alaska Region: Tectonophysics, v. 497, p. 105–113, https://doi.org/10.1016/j.tecto.2010.10.019.

Dumoulin, J.A., 1988, Sandstone petrographic evidence and the Chugach–Prince William terrane boundary in southern Alaska: Geology, v. 16, p. 456–460, https://doi.org/10.1130/0091-7613(1988)016<0456:SPEATC>2.3.CO;2.

Dunn, C.A., Enkelmann, E., Ridgway, K.D., and Allen, W.K., 2017, Source to sink evaluation of sediment routing in the Gulf of Alaska and Southeast Alaska: A thermochronometric perspective: Journal of Geophysical Research: Earth Surface, v. 122, p. 711–734, https://doi.org/10.1002/2016JF004168.

Dusel-Bacon, C., Csejtey, B., Foster, H.L., Doyle, E.O., Nokleberg, W.J., and Plafker, G., 1993, Distribution, facies, ages, and proposed tectonic associations of regionally metamorphosed rocks in east- and south-central Alaska: U.S. Geological Survey Professional Paper 1497C, 80 p., https://doi.org/10.3133/pp1497C.

Eberhart-Phillips, D., et al., 2003, The 2002 Denali fault earthquake, Alaska: A large magnitude, slip-partitioned event: Science, v. 300, p. 1113–1118, https://doi.org/10.1126/science.1082703.

Ehlers, T.A., Szameitat, A., Enkelmann, E., Yanites, B.J., and Woodsworth, G.J., 2015, Identifying spatial variations in glacial catchment erosion with detrital thermochronology: Journal of Geophysical Research: Earth Surface, v. 120, p. 1023–1039, https://doi.org/10.1002/2014JF003432.

Eisbacher, G., 1976, Sedimentology of the Dezadeash flysch and its implications for strike-slip faulting along the Denali fault, Yukon Territory and Alaska: Canadian Journal of Earth Sciences, v. 13, no. 11, p. 1495–1513, https://doi.org/10.1139/e76-157.

Eisbacher, G., and Hopkins, S., 1977, Mid-Cenozoic paleogeomorphology and tectonic setting of the St. Elias Mountains, Yukon Territory: Geological Survey of Canada Paper 77, p. 319–335, https://doi.org/10.4095/102804.

Elliott, J.L., Larsen, C.F., Freymueller, J.T., and Motyka, R.J., 2010, Tectonic block motion and glacial isostatic adjustment in southeast Alaska and adjacent Canada constrained by GPS measurements: Journal of Geophysical Research: Solid Earth, v. 115, B09407, https://doi.org/10.1029/2009JB007139.

Engebretson, D.C., Cox, A., and Gordon, R.G., 1985, Relative motions between oceanic and continental plates in the Pacific Basin: Geological Society of America Special Paper 206, 59 p., https://doi.org/10.1130/SPE206.

Enkelmann, E., and Ehlers, T.A., 2015, Evaluation of detrital thermochronology for quantification of glacial catchment denudation and sediment mixing: Chemical Geology, v. 411, p. 299–309, https://doi.org/10.1016/j.chemgeo.2015.07.018.

Enkelmann, E., Garver, J.I., and Pavlis, T.L., 2008, Rapid exhumation of ice-covered rocks of the Chugach–St. Elias orogen, SE-Alaska: Geology, v. 36, p. 915–918, https://doi.org/10.1130/G2252A.1.

Enkelmann, E., Zeitler, P.K., Pavlis, T.L., Garver, J.I., and Ridgway, K.D., 2009, Intense localized rock uplift and erosion in the St. Elias orogen of Alaska: Nature Geoscience, v. 2, p. 360–363, https://doi.org/10.1038/ngeo502.

Enkelmann, E., Zeitler, P.K., Garver, J.I., Pavlis, T.L., and Hooks, B.P., 2010, The thermochronological record of tectonic and surface process interaction at the Yakutat–North American collision zone in southeast Alaska: American Journal of Science, v. 310, p. 231–260, https://doi.org/10.2475/04.2010.01.

Enkelmann, E., Koons, P.O., Pavlis, T.L., Hallet, B., Barker, A., Elliott, J., Garver, J.I., Gulick, S.P.S., Headley, R.M., Pavlis, G.L., Ridgway, K.D., Ruppert, N., and van Avendonk, H., 2015a, Cooperation of tectonic and surface processes produces Earth's highest coastal mountains: Geophysical Research Letters, v. 42, p. 5838–5846, https://doi.org/10.1002/2015GL064727.

Enkelmann, E., Valla, P.G., and Champagnac, J.-D., 2015b, Low-temperature thermochronology of the Yakutat plate corner, St. Elias Range (Alaska): Bridging short-term and long-term deformation: Quaternary Science Reviews, v. 113, p. 23–38, https://doi.org/10.1016/j.quascirev.2014.10.019.

Enkelmann, E., Piestrzeniewicz, A., Falkowski, S., Stübner, K., and Ehlers, T.A., 2017, Thermochronology in southeast Alaska and southwest Yukon: Implications for North American Plate response to terrane accretion: Earth and Planetary Science Letters, v. 457, p. 348–358, https://doi.org/10.1016/j.epsl.2016.10.032.

Enkelmann, E., Sanchez Lohff, S.K., and Finzel, F.S., 2019, Detrital zircon double-dating of forearc basin strata reveals magmatic, exhumational, and thermal history of sediment source areas: Geological Society of America Bulletin, v. 131, no. 7/8, p. 1364–1384, https://doi.org/10.1130/B35043.1.

Erdmer, P., and Mortensen, J.K., 1993, A 1200-km-long Eocene metamorphic-plutonic belt in the northwestern Cordillera: Evidence from southwest Yukon: Geology, v. 21, p. 1039–1042, https://doi.org/10.1130/0091-7613(1993)021<1039:AKLEMP>2.3.CO;2.

Falkowski, S., and Enkelmann, E., 2016, Upper-crustal cooling of the Wrangellia composite terrane in the northern St. Elias Mountains, western Canada: Lithosphere, v. 8, no. 4, p. 359–378, https://doi.org/10.1130/L508.1.

Falkowski, S., Enkelmann, E., and Ehlers, T.A., 2014, Constraining the area of rapid and deep-seated exhumation at the St. Elias syntaxis, Southeast Alaska, with detrital zircon fission-track analysis: Tectonics, v. 33, p. 597–616, https://doi.org/10.1002/2013TC003408.

Falkowski, S., Enkelmann, E., Drost, K., Pfänder, J.A., Stübner, K., and Ehlers, T.A., 2016, Cooling history of the St. Elias syntaxis, southeast Alaska, revealed by geo- and thermochronology of cobble-size glacial detritus: Tectonics, v. 35, p. 447–468, https://doi.org/10.1002/2015TC004086.

Farmer, G.L., Ayuso, R., and Plafker, G., 1993, A Coast Mountains provenance for the Valdez and Orca groups, southern Alaska, based on Nd, Sr, and Pb isotopic evidence: Earth and Planetary Science Letters, v. 116, p. 9–21, https://doi.org/10.1016/0012-821X(93)90042-8.

Farrar, E., Clark, A.H., Archibald, D.A., and Way, D.C., 1988, Potassium-argon age of granitoid pluton rocks, southwest Yukon Territory, Canada: Isochron/West, v. 51, p. 19–23.

Finzel, E.S., Trop, J.M., Ridgway, K.D., and Enkelmann, E., 2011, Upper plate proxies for flat-slab subduction processes in southern Alaska: Earth and Planetary Science Letters, v. 303, p. 348–360, https://doi.org/10.1016/j.epsl.2011.01.014.

Fitzgerald, P.G., Sorkhabi, R.B., Redfield, T.F., and Stump, E., 1995, Uplift and denudation of the central Alaska Range: A case study in the use of apatite fission track thermochronology to determine absolute uplift parameters: Journal of Geophysical Research: Solid Earth, v. 100, p. 20,175–20,191, https://doi.org/10.1029/95JB02150.

Fitzgerald, P.G., Roeske, S.M., Benowitz, J.A., Riccio, S.J., Perry, S.E., and Armstrong, P.A., 2014, Alternating asymmetric topography of the Alaska Range along the strike-slip Denali fault: Strain partitioning and lithospheric control across a terrane suture zone: Tectonics, v. 33, p. 1519–1533, https://doi.org/10.1002/2013TC003432.

Garrity, C.P., and Soller, D.R., 2009, Database of the Geologic Map of North America; adapted from the Map by J.C. Reed, Jr., and others (2005): U.S. Geological Survey Data Series 424, https://doi.org/10.3133/ds424.

Garver, J.I., Brandon, M.T., Roden-Tice, M., and Kamp, P.J.J., 1999, Exhumation history of orogenic highlands determined by detrital fission-track thermochronology, *in* Ring, U., Brandon, M.T., Lister, G.S., and Willett, S.D., eds., Exhumation Processes: Normal Faulting, Ductile Flow and Erosion: Geological Society, London, Special Publication 154, p. 283–304, https://doi.org/10.1144/GSL.SP.1999.154.01.13.

Gasser, D., Bruand, E., Stüwe, K., Foster, D.A., Schuster, R., Fügenschuh, B., and Pavlis, T., 2011, Formation of a metamorphic complex along an obliquely convergent margin: Structural and thermochronological evolution of the Chugach Metamorphic Complex, southern Alaska: Tectonics, v. 30, TC2012, https://doi.org/10.1029/2010TC002776.

Gehrels, G.E., 2000, Reconnaissance geology and U-Pb geochronology of the western flank of the Coast Mountains between Juneau and Skagway, southeastern Alaska, *in* Stowell, H.H., and McClelland, W.C., eds., Tectonics of the Coast Mountains, Southeastern Alaska and British Columbia: Geological Society of America Special Paper 343, p. 213–234, https://doi.org/10.1130/0-8137-2343-4.213.

Grabowski, D., Enkelmann, E., and Ehlers, T.A., 2013, Spatial extent of rapid exhumation in the St. Elias syntaxis region, SE Alaska: Journal of Geophysical Research: Earth Surface, v. 118, p. 1921–1938, https://doi.org/10.1002/jgrf.20136.

Haeussler, P.J., Bradley, D.C., Wells, R.E., and Miller, M.L., 2003, Life and death of the Resurrection plate: Evidence for its existence and subduction in the northeastern Pacific in Paleocene–Eocene time: Geological Society of America Bulletin, v. 115, no. 7, p. 867–880, https://doi.org/10.1130/0016-7606(2003)115<0867:LADOTR>2.0.CO;2.

Haeussler, P.J., Matmon, A., Schwartz, D.P., and Seitz, G.G., 2017, Neotectonics of interior Alaska and the late Quaternary slip rate along the Denali fault system: Geosphere, v. 13, p. 1445–1463, https://doi.org/10.1130/GES01447.1.

Hudson, T., and Plafker, G., 1982, Paleogene metamorphism of an accretionary flysch terrane, eastern Gulf of Alaska: Geological Society of America Bulletin, v. 93, p. 1280–1290, https://doi.org/10.1130/0016-7606(1982)93<1280:PMOAAF>2.0.CO;2.

Hudson, T., Plafker, G., and Lanphere, M.A., 1977, Intrusive rocks of the Yakutat–St. Elias area, south-central Alaska: Journal of Research of the U.S. Geological Survey, v. 5, p. 155–172.

Hurford, A.J., 1990, Standardization of fission track dating calibration: Recommendation by the Fission Track Working Group of the I.U.G.S: Subcommission on Geochronology: Chemical Geology: Isotope Geoscience Section, v. 80, p. 171–178, https://doi.org/10.1016/0168-9622(90)90025-8.

Ingram, G.M., and Hutton, D.H., 1994, The Great Tonalite Sill: Emplacement into a contractional shear zone and implications for Late Cretaceous to early Eocene tectonics in southeastern Alaska and British Columbia: Geological Society of America Bulletin, v. 106, p. 715–728, https://doi.org/10.1130/0016-7606(1994)106<0715:TGTSEI>2.3.CO;2.

Israel, S., Beranek, L., Friedman, R.M., and Crowley, J.L., 2014, New ties between the Alexander terrane and Wrangellia and implications for North American Cordilleran evolution: Lithosphere, v. 6, p. 270–276, https://doi.org/10.1130/L364.1.

Israel, S.A., Murphy, D., Bennett, V., Mortensen, J., and Crowley, J.L., 2011, New insight into the geology and mineral potential of the Coast Belt in southwestern Yukon, *in* Mac-Farlane, K.E., et al., eds., Yukon Exploration and Geology 2010: Whitehorse, Yukon Territory, Canada, Yukon Geological Survey, p. 101–123.

Jones, D.L., Irwin, W.P., and Ovenshine, A.T., 1972, Southeastern Alaska—A displaced continental fragment?: U.S. Geological Survey Professional Paper 800B, p. B211–B217.

Kalbas, J.L., Freed, A.M., and Ridgway, K.D., 2008, Contemporary fault mechanics in southern Alaska, *in* Freymueller, J.T., Haeussler, P.J., Wesson, R.L., and Ekström, G., eds., Active Tectonics and Seismic Potential of Alaska: Washington, D.C., American Geophysical Union, Geophysical Monograph Series, v. 179, p. 321–336, https://doi.org/10.1029/179GM18.

Ketcham, R.A., Donelick, R.A., and Carlson, W.D., 1999, Variability of apatite-fission-track annealing kinetics. III. Extrapolation to geological time scales: The American Mineralogist, v. 84, p. 1235–1255, https://doi.org/10.2138/am-1999-0903.

Koehler, R.D., Farrell, R.-E., Burns, P.A., and Combellick, R.A., 2012, Quaternary faults and folds in Alaska: A digital database, *in* Koehler, R.D., ed., Quaternary Faults and Folds (QFF): Alaska Division of Geological and Geophysical Surveys Miscellaneous Publication 141, scale 1:3,700,00, 1 sheet, 31 p. text, https://doi.org/10.14509/23944.

Lease, R.O., Haeussler, P.J., and O'Sullivan, P.B., 2016, Changing exhumation patterns during Cenozoic growth and glaciation of the Alaska Range: Insights from detrital thermochronology and geochronology: Tectonics, v. 35, p. 934–955, https://doi.org/10.1002/2015TC004067.

Lease, R.O., Haeussler, P.J., Witter, R.C., Stockli, D.F., Bender, A.M., Kelsey, H.M., and O'Sullivan, P.B., 2021, Extreme Quaternary plate boundary exhumation and strike slip localized along the southern Fairweather fault, Alaska, USA: Geology, v. 49, p. 602–606, https://doi.org/10.1130/G48464.1.

Lowey, G.W., 1992, Variation in bed thickness in a turbidite succession, Dezadeash Formation (Jurassic–Cretaceous), Yukon, Canada: Evidence of thinning upward and thickening-upward cycles: Sedimentary Geology, v. 78, p. 217–232, https://doi.org/10.1016/0037-0738(92)90021-I.

Lowey, G.W., 1998, A new estimate of the amount of displacement on the Denali fault system based on the occurrence of carbonate megaboulders in the Dezadeash Formation (Jura-Cretaceous), Yukon, and the Nutzotin Mountains sequence (Jura-Cretaceous), Alaska: Bulletin of Canadian Petroleum Geology, v. 46, p. 379–386.

Lowey, G.W., 2000, The Tatshenshini shear zone (new) in southwestern Yukon, Canada: Comparison with the coast shear zone in British Columbia and southeastern Alaska and implications regarding the Shakwak suture: Tectonics, v. 19, no. 3, p. 512–528, https://doi.org/10.1029/1999TC001119.

Marechal, A., Mazzotti, S., Elliott, J.L., Freymueller, J.T., and Schmidt, M., 2015, Indentor-corner tectonics in the Yakutat-St. Elias collision constrained by GPS: Journal of Geophysical Research: Solid Earth, v. 120, p. 3897–3908, https://doi.org/10.1002/2014JB011842.

Marechal, A., Ritz, J.-F., Ferry, M., Mazzotti, S., Blard, P.-H., Braucher, R., and Saint-Carlier, D., 2018, Active tectonics around the Yakutat indentor: New geomorphological constraints on the eastern Denali, Totschunda and Duke River Faults: Earth and Planetary Science Letters, v. 482, p. 71–80, https://doi.org/10.1016/j.epsl.2017.10.051.

McAleer, R.J., Spotila, J.A., Enkelmann, E., and Berger, A.L., 2009, Exhumation along the Fairweather Fault, southeastern Alaska, based on low-temperature thermochronometry: Tectonics, v. 28, TC1007, https://doi.org/10.1029/2007TC002240.

McDermott, R.G., Ault, A.K., Caine, J.S., and Thomson, S.N., 2019, Thermotectonic history of the Kluane Ranges and evolution of the eastern Denali fault zone in southwestern Yukon, Canada: Tectonics, v. 38, p. 2983–3010, https://doi.org/10.1029/2019TC005545.

Meigs, A.J., Johnston, S., Garver, J.I., and Spotila, J.A., 2008, Crustal-scale structural architecture, shortening, and exhumation of an active, eroding orogenic wedge (Chugach/St. Elias Range, southern Alaska): Tectonics, v. 27, TC4003, https://doi.org/10.1029/2007TC002168.

Miller, M.L., Bradley, D.C., Bundtzen, T.K., and McClelland, W., 2002, Late Cretaceous through Cenozoic strike-slip tectonics of southwestern Alaska: The Journal of Geology, v. 110, no. 3, p. 247–270, https://doi.org/10.1086/339531.

Nokleberg, W.J., Jones, D.L., and Silberling, N.J., 1985, Origin and tectonic evolution of the Maclaren and Wrangellia terranes, eastern Alaska Range, Alaska: Geological Society of America Bulletin, v. 96, p. 1251–1270, https://doi.org/10.1130/0016-7606(1985)96<1251:OATEOT>2.0.CO;2.

Nokleberg, W.J., Plafker, G., and Wilson, F.H., 1994, Geology of south-central Alaska, *in* Plafker, G., and Berg, H.C., eds., The Geology of Alaska: Boulder, Colorado, USA, Geological Society of America, Geology of North America, v. G-1, p. 311–366.

O'Sullivan, P.B., and Currie, L.D., 1996, Thermotectonic history of Mt. Logan, Yukon Territory, Canada: Implications of multiple episodes of Middle to Late Cenozoic denudation: Earth and Planetary Science Letters, v. 144, p. 251–261, https://doi.org/10.1016/0012-821X(96)00161-6.

O'Sullivan, P.B., Plafker, G., and Murphy, J.M., 1997, Apatite fission-track thermotectonic history of crystalline rocks in the northern St. Elias Mountains, Alaska, *in* Dumoulin, J.A., and Gray, J.E., eds., Geological Studies in Alaska by the U.S. Geological Survey, 1996: U.S. Geological Survey Professional Paper 1574, p. 283–294.

Pavlis, T.L., and Roeske, S.M., 2007, The Border Ranges fault system, southern Alaska: Geological Society of America Bulletin, v. 431, p. 95–127, https://doi.org/10.1130/2007.2431(05).

Pavlis, T.L., Chapman, J.B., Bruhn, R.L., Ridgway, K., Worthington, L.L., Gulick, S.P., and Spotila, J., 2012, Structure of the actively deforming fold-thrust belt of the St. Elias orogen with implications for glacial exhumation and three-dimensional tectonic processes: Geosphere, v. 8, p. 991–1019, https://doi.org/10.1130/GES00753.1.

Plafker, G., 1987, Regional geology and petroleum potential of the northern Gulf of Alaska continental margin, *in* Scholl, D.W., et al., eds., Geology and Resource Potential of the Continental Margin of Western North America and Adjacent Ocean Basins: Houston, Texas, Circum-Pacific Council for Energy and Mineral Resources, Earth Science Series, v. 6, p. 229–268.

Plafker, G., Moore, J.C., and Winkler, G.R., 1994, Geology of the southern Alaska margin, *in* Plafker, G., and Berg, H.C., eds., The Geology of Alaska: Boulder, Colorado, USA, Geological Society of America, The Geology of North America, v. G-1, p. 389–449.

Plattner, C., Malservisi, R., Dixon, T.H., LaFemina, P., Sella, G.F., Fletcher, J., and Suarez-Vidal, F., 2007, New constraints on relative motion between the Pacific Plate and Baja California microplate (Mexico) from GPS measurements: Geophysical Journal International, v. 170, p. 1373–1380, https://doi.org/10.1111/j.1365-246X.2007.03494.x.

Power, M.A., 1988, Microearthquake seismicity on the Duke River, Denali Fault system, *in* Abbott, J.G., ed., Yukon Geology, v. 2: Yukon, Canada, Exploration & Geological Services Division, Indian & Northern Affairs Canada, p. 61–68.

Regan, S.P., Benowitz, J.A., and Holland, M.E., 2020, A plutonic brother from another magma mother: Disproving the Eocene Foraker-McGonagall pluton piercing point and implications for long-term slip on the Denali Fault: Terra Nova, v. 32, p. 66–74, https://doi.org/10.1111/ter.12437.

Riccio, S.J., Fitzgerald, P.G., Benowitz, J.A., and Roeske, S.M., 2014, The role of thrust faulting in the formation of the eastern Alaska Range: Thermochronological constraints from the Susitna Glacier thrust fault region of the intracontinental strike-slip Denali fault system: Tectonics, v. 33, p. 2195–2217, https://doi.org/10.1002/2014TC003646.

Richter, D., Smith, J.G., Lanphere, M., Dalrymple, G., Reed, B., and Shew, N., 1990, Age and progression of volcanism, Wrangell volcanic field, Alaska: Bulletin of Volcanology, v. 53, p. 29–44, https://doi.org/10.1007/BF00680318.

Ridgway, K., DeCelles, P., Cameron, A., and Sweet, A., 1992, Cenozoic syntectonic sedimentation and strike-slip basin development along the Denali fault system, Yukon Territory: Yukon Geology, v. 3, p. 1–26.

Ridgway, K.D., and DeCelles, P.G., 1993a, Petrology of Mid-Cenozoic strike-slip basins in an accretionary orogen, St. Elias Mountains, Yukon Territory, Canada, *in* Johnsson, M.J., and Basu, A., eds., Processes Controlling the Composition of Clastic Sediments: Geological Society of America Special Paper 284, https://doi.org/10.1130/SPE284-p67.

Ridgway, K.D., and DeCelles, P.G., 1993b, Stream-dominated alluvial fan and lacustrine depositional systems in Cenozoic strike-slip basins, Denali fault system, Yukon Territory, Canada: Sedimentology, v. 40, no. 4, p. 645–666, https://doi.org/10.1111/j.1365-3091.1993.tb01354.x.

Ridgway, K.D., Trop, J.M., Nokleberg, W.J., Davidson, C.M., and Eastham, K.R., 2002, Mesozoic and Cenozoic tectonics of the eastern and central Alaska Range: Progressive basin development and deformation in a suture zone: Geological Society of America Bulletin, v. 114, p. 1480–1504, https://doi.org/10.1130/0016-7606(2002)114<1480:MACTOT>2.0.CO;2.

Rubin, C.M., Saleeby, J.B., Cowan, D.S., Brandon, M.T., and McGroder, M.F., 1990, Regionally extensive mid-Cretaceous west-vergent thrust system in the northwestern Cordillera: Implications for continent-margin tectonism: Geology, v. 18, p. 276–280, https://doi.org/10.1130/0091-7613(1990)018<0276:REMCWV>2.3.CO;2.

Schartman, A., Enkelmann, E., Garver, J.I., and Davidson, C., 2019, Uplift and Exhumation of the Russell Fiord and Boundary blocks along the northern Fairweather Transform Fault, Alaska: Lithosphere, v. 11, p. 232–251, https://doi.org/10.1130/L1011.1.

Shugar, D., Clague, J.J., Best, J.L., Schoof, C., Willis, M.J., Copland, L., and Roe, G.H., 2017, River piracy and drainage basin reorganization led by climate-driven glacier retreat: Nature Geoscience, v. 10, p. 370–375, https://doi.org/10.1038/ngeo2932.

Skulski, T., Francis, D., and Ludden, J., 1991, Arc-transform magmatism in the Wrangell volcanic belt: Geology, v. 19, p. 11–14, https://doi.org/10.1130/0091-7613(1991)019<0011:ATMITW>2.3.CO;2.

Skulski, T., Francis, D., and Ludden, J., 1992, Volcanism in an arc-transform transition zone: The stratigraphy of the St. Clare Creek volcanic field, Wrangell volcanic belt, Yukon, Canada: Canadian Journal of Earth Sciences, v. 29, no. 3, p. 446–461, https://doi.org/10.1139/e92-039.

Spotila, J.A., and Berger, A.L., 2010, Exhumation at orogenic indentor corner under long-term glacial conditions: Example of the St. Elias orogen, southern Alaska: Tectonophysics, v. 490, p. 241–256, https://doi.org/10.1016/j.tecto.2010.05.015.

Spotila, J.A., Buscher, J.T., Meigs, A.J., and Reiners, P.W., 2004, Long-term glacial erosion of active mountain belts: Example of the Chugach-St. Elias Range, Alaska: Geology, v. 32, p. 501–504, https://doi.org/10.1130/G20343.1.

Stevens, R.D., Delabio, R.N., and Lachance, G.R., 1982, Age Determinations and Geological Studies: K-Ar Isotopic Ages, Report 15: Geological Survey of Canada Paper 81-2, 56 p.

Trop, J.M., Hart, W.K., Snyder, D., and Idleman, B., 2012, Miocene basin development and volcanism along a strike-slip to flat-slab subduction transition: Stratigraphy, geochemistry, and geochronology of the central Wrangell volcanic belt, Yakutat–North America collision zone: Geosphere, v. 8, p. 805–834, https://doi.org/10.1130/GES00762.1.

Vermeesch, P., 2004, How many grains are needed for a provenance study?: Earth and Planetary Science Letters, v. 224, p. 441–541, https://doi.org/10.1016/j.epsl.2004.05.037.

Wilson, F.H., Hults, C.P., Mull, C.G., and Karl, S.M., compilers, 2015, Geologic map of Alaska: U.S. Geological Survey Scientific Investigations Map 3340, scale 1:1,584,000, 2 sheets, 196 p. text, https://doi.org/10.3133/sim3340.

Worthington, L.L., Van Avendonk, H.J., Gulick, S.P., Christeson, G.L., and Pavlis, T.L., 2012, Crustal structure of the Yakutat Terrane and the evolution of subduction and collision in southern Alaska: Journal of Geophysical Research: Solid Earth, v. 117, B01102, https://doi.org/10.1029/2011JB008493.